Validation Of A Seat-Dummy Simulation Model For Rear-Impact

Thomas Deter (Author)
IAT
Axel Malczyk
Matthias Kuehn
German Insurance Association – Accident Research
Germany
Paper Number 07-0151

ABSTRACT

Seat test standard protocols have been established by insurance research institutes and consumer test organisations are developing similar test procedures to assess the performance of seats under rear-impact crash conditions.
With several numerical simulation models of the BioRID II being commercially available this study is intended to validate a multi-body rear-impact dummy model in a neutral seat environment for a range of seating postures and impact severities. This enables the systematic investigation of those parameters of the seat which influence the biomechanical loading on the dummy.
For this purpose, five dynamic tests were conducted on a newly developed test device that employs a stationary carriage with the seat and dummy and is accelerated from the rear by a sled-on-carriage impactor system. The BioRID dummy was placed on the so-called Chalmers seat which was utilized in earlier EU co-funded research projects and provides several adjustment possibilities to represent different seat shapes and characteristics. Starting with a medium severity crash pulse four additional validation tests were carried out with lower and higher crash severity as well as different seat and seating positions to cover a broader range of conditions.
Modelling involved both the detailed measuring and computational representation of the Chalmers seat as a multi-body model with facet surfaces as well as careful documentation of the placement of the BioRID model on the seat.
Based on the comparison of the model response with the kinematics and biomechanical measurements from the basic test an acceptable conformity between numerical model and validation test could be found for most body regions. However, some shortcomings in the dummy model were identified.

INTRODUCTION

Soft tissue neck injuries, often termed whiplash-associated disorders, are among the most frequently reported injuries of car occupants in many countries with a high level of motorization [1]. Although assessed as minor injures and usually healing without further bodily impairment they represent a large burden to society due to the large number of incidents, mostly among occupants of passenger cars struck in the rear by another vehicle. A comparative study conducted by the European insurance industry in 2004 reported a large difference in the situation of minor cervical trauma claims among European countries, both in number of claims and in cost of injury [2]. For instance, in Germany approximately 47% of all bodily injury claims are linked only to minor neck injuries, for France this rate is only 3% and for the United Kingdom it is approximately 76%. The annual costs of these injuries range from an estimated 1.5 million Euros in Finland to 500 million in Germany to more than 2.9 billion Euros in Italy. Many research studies have investigated into the injury mechanisms and have tried to establish biomechanical threshold values for these types of injuries, but a common understanding does not exist until today. The International Insurance Whiplash Prevention Group (IIWPG), a group of insurance research institutes from North America, Australia and Europe developed a geometric and dynamic test and assessment protocol for car seats [3]. This formed the basis for test programs of new vehicle seats which have been published for three years in a row to inform consumers and to increase the awareness in the automotive industry about the safety performance of seats under rear-impact conditions. The assessment criteria employed in this protocol have their foundation in surveys of the number of neck injury claims in connection with particular passenger car models [4]. For two vehicle models, the number of claims for the model generation equipped with standard seats was compared with the claim figures for the subsequent generation which featured seat

designs specifically engineered for better rear-impact neck protection. Employing the BioRID II anthropometric test device, laboratory tests with these seats under rear-impact conditions displayed significant differences in some biomechnical variables depending on the design strategy against neck injury. While all of them aim at reducing the upper neck forces (shear and axial) the methods differ. Specifically energy-absorbing seat backs reduce the longitudinal acceleration in the T1 vertebra of the BioRID II dummy whereas re-active head restraints seek to minimize the time to close the gap to the back of the head. These physical values serve as seat evalution criteria in the IIWPG test procedure. While a considerable number of passenger car front seats has been evaluated according to this protocol it still requires physical testing. Some dummy responses have shown to be sensitive to slight variations in seating position and seat variability as it may occur in serial production. Moreover, the interaction between dummy and seat is often difficult to observe since the view can be obstructed by the dummy's arms, clothing or the seat upholstery.
This was the major motivation to develop a validated numerical simulation model which includes a commercially available BioRID II model in a neutral seat environment. Such a model would enable to study the influence of a variety of seat and impact parameters on the dummy loadings with special focus on the cervical and thoracic spine. Numerical simulation can also serve as a cost-efficient and time-saving alternative to testing when fundamental effects of other seat types, e.g., for light commercial vehicles or rear seat benches, need to be investigated. Hence, great store was set by the prognostic capabilites of the numerical model for a range of possible dummy seating positions and impact severities.

VALIDATION TESTING

Development of Dynamic Test Device

Experience from other laboratory experiments shows that the initial dummy position has large influence on the result of a dynamic rear-impact test. Therefore, the objective was to design a test set-up with a stationary carriage which is accelerated when the crash pulse sets in. A Hyge sled was not available for testing. Instead, a system was developed where the seat is mounted on a stationary carriage which is accelerated from the rear by an impactor device with a defined crash pulse. Sets of coil springs are used to transfer the impact forces which enhances the repeatibility of the force characteristics between tests and reduces test costs.
The concept was worked out using a MADYMO simulation model of the test set-up. The first evaluations of a system which employed a single impacting mass revealed that this would permit only the realisation of harmonic crash pulses. In order to simulate crash characteristics of non-harmonic shape like the IIWPG crash pulse an additional mass is necessary to interact with the seat carriage at a later point in time during the impact. A similar effect was achieved with the development of a sled-on-carriage system, incorporating the impactor carriage and an additional sliding mass. By adjusting the amount of additional mass, the time that it interacts with the seat carriage and the stiffness of the coil springs the crash pulse can be tuned to the desired shape. Different options of setting-up the additional masses on the impactor carriage were investigated. A simple lumped mass model with coil springs was used to determine a suitable combination of mass and spring stiffnesses. However, no masses were assigned to the springs in the model. The schematic test set-up is shown in Figure 1.

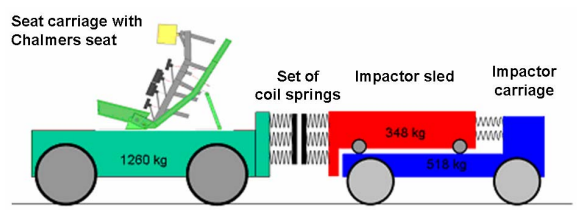

Figure 1. Schematic test set-up.

During the first pre-tests with a physical test device it became clear that the natural oscillation of the spring coils has significant influence on the resulting crash pulse. The MADYMO model was therefore refined in the area of the spring simulation. Each coil spring was modelled as a system consisting of ten bodies with linear stiffnesses in between. The large number of springs resulted in a complex calculation model, but with good prognostic capability. By distributing the springs among the impactor sled and the seat carriage their effect on the crash pulse could be greatly reduced.

Figure 2. Sets of coil springs between impactor sled and seat carriage.

Figure 3 shows the target crash pulse, the IIWPG curve in this case, in comparison with the calculated pulse and the pulse measured in the experiment. The corridor defined by IIWPG is met except for a slight deviation in the time frame after 87 milliseconds.

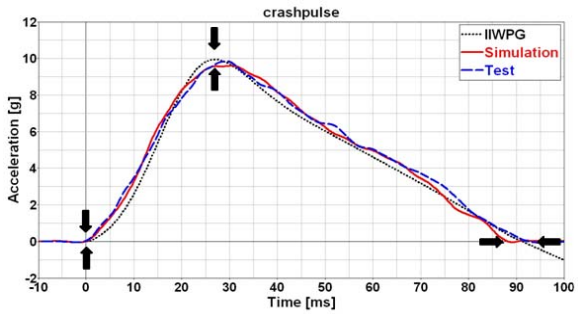

Figure 3. Comparison of IIWPG target pulse, calculated and test crash pulse.

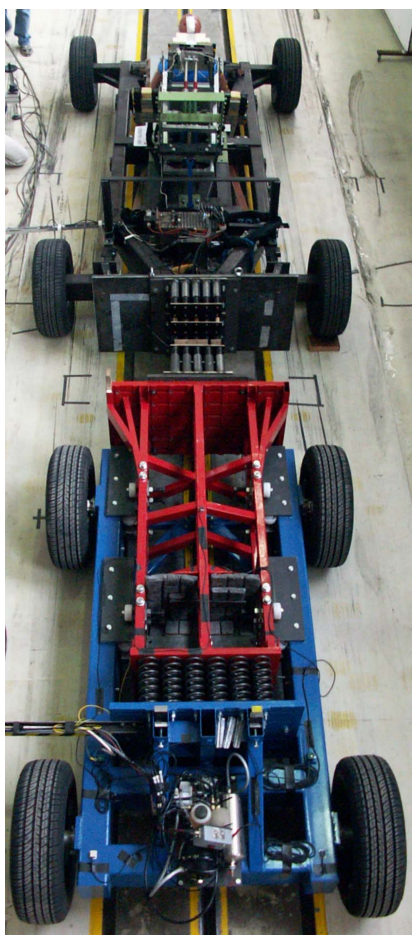

Figure 4. Complete test set-up with impactor (foreground) and seat carriage (background).

Test Seat

For the primarily intended purpose of a parameter study the use of production car seats entails some disadvantages. The observation of the interaction between dummy and the seat is limited due to upholstery, especially on the seat cushion and seat back sides. Purposeful variation of seat parameters requires extensive modifications of the seat construction and may alter its performance unintentionally. For this reason, the so-called Chalmers seat was used in the dynamic validation tests. It was developed in the course of the „Whiplash“ project co-funded by the EC [5] and was employed in several research projects focussing on rear-impact neck injury and protection. This seat displays a generic design with a number of separate and adjustable seat elements which allows a detailed investigation of the interaction between dummy and seat and the variation of isolated seat parameters.

The seat features a rigid seating surface and an adjustable seat back frame with an articulated sub-frame which carries four movable seat back elements and a movable head restraint (see Figure 5 and 6). All of the seat back elements and the head restraint can be individually adjusted. The sub-frame is connected to the seat back frame by means of a deformation element that works according to the principle of a sheet metal bending brake.

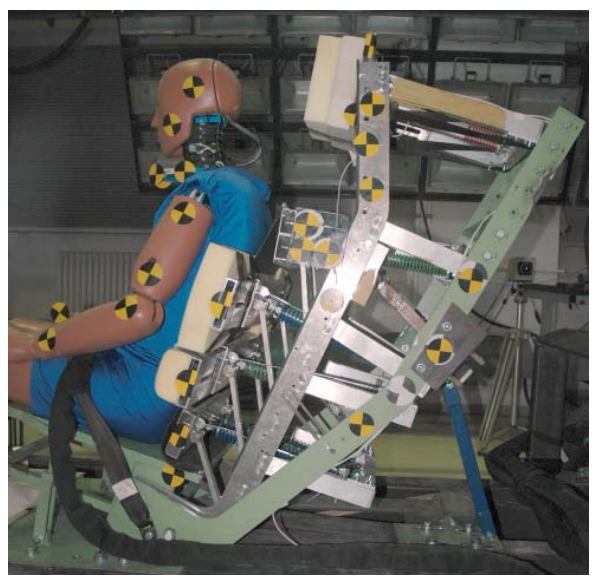

Figure 5. Chalmers seat.

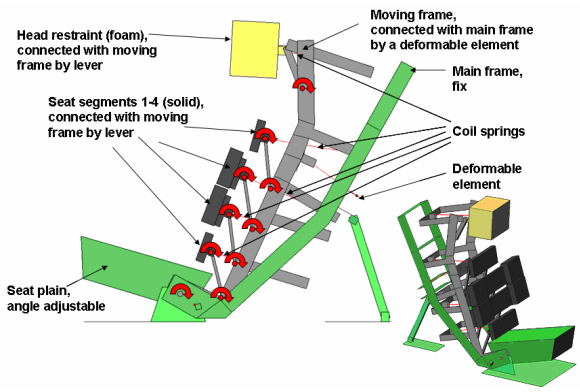

Figure 6. Schematic representation of Chalmers Seat.

Validation Tests

A large number of characteristic points on the dummy and on the seat were measured before the tests to obtain detailed data for the following set-up of the numerical simulation model and to ensure a repeatable dummy position for all tests (see Figure 7). The tests were documented with three high-speed video cameras. On the seat carriage, the longitudinal acceleration was measured and signals on all standard measurement locations of the BioRID II dummy were recorded and processed according to SAE standards (see Figure 8).
The test dummy was freshly calibrated before the test series and conditions of the test environment met IIWPG requirements. This provided an extensive amount of information and measurement data from the validation tests for the development of a numerical simulation model.
Altogether, five validation tests were conducted with the described test set-up and using the BioRID II anthropometric test device: a basic test applying the IIWPG crash pulse, one test each with reduced and increased crash severity, one test with increased backset between dummy head and head restraint and one test with increased seat back angle.

Test No.	Description
V01	Increased backset
V02	Basic test conditions
V03	Reduced crash severity
V04	Increased seat back angle
V05	Increased crash severity

Starting from the basic test conditions, the purpose was to vary the crash pulse severity in two tests and maintain the remaining parameters, and to vary the seat geometry in two tests while maintaining all other parameters. The initial positioning of the test dummy was carried out according to IIWPG requirements as far as the Chalmers seat design allowed; the seating position was then replicated for the tests with variation of the crash pulse. In the tests with increased backset and with reclined seat back, the dummy posture had to be changed slightly to achieve the desired seat adjustments.

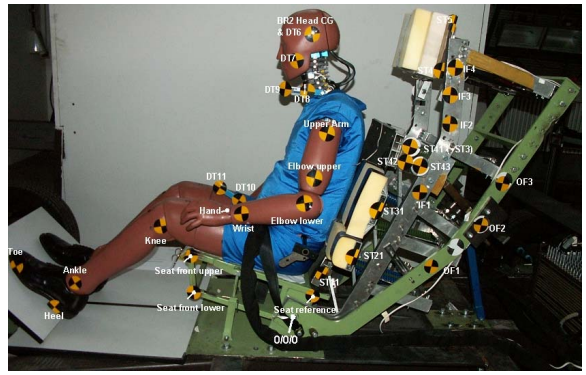

Figure 7. Measurement points on dummy and test device.

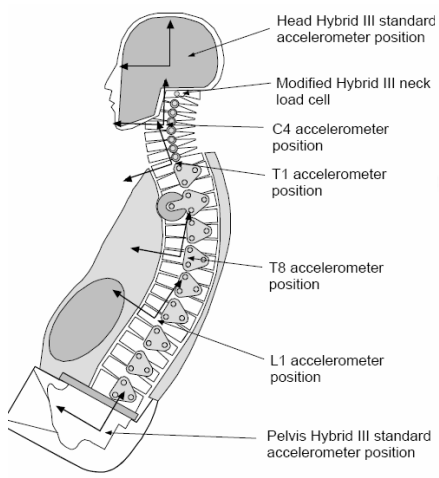

Figure 8. Measurement locations on BioRID II dummy.

The test results were assessed largely in accordance with IIWPG guidelines. The maximum shear and axial forces measured on the upper neck are represented in a rating chart as used by IIWPG to classify the combined neck force values according to one of the three categories of “low”, “moderate” and “high” neck forces (see Figure 10). Similarly, the maximum longitudinal acceleration measured on the T1 thoracic vertebra is assessed when rating the performance of seats under rear-impact conditions.

Effect of Crash Severity

In three of the validation tests, the crash severity was varied whereas all other variables remained unchanged. Starting from the crash pulse in base test

V02, representing the IIWPG condition, a pulse of lower severity with a peak acceleration of 8 g's and a pulse of higher severity with almost 13 g's were applied. Their corresponding delta v's total 13.0 kph and 17.6 kph, respectively.

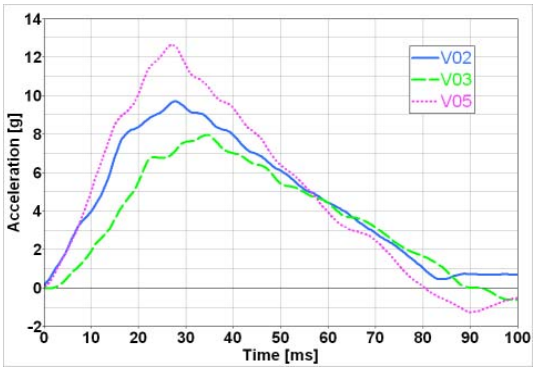

Figure 9. Different crash pulses used for validation tests.

The following figures show the effect of crash severity on dummy loadings according to IIWPG. However, the present study takes into consideration also negative shear values for illustration in the rating chart and assessment of the validation quality.

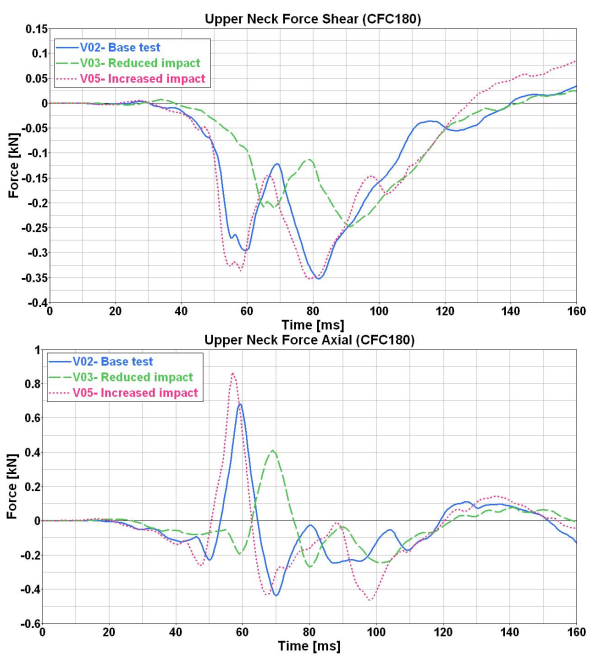

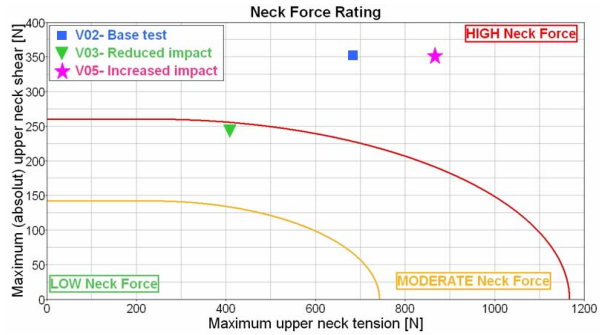

Figure 10. Effect of crash severity on upper neck forces.

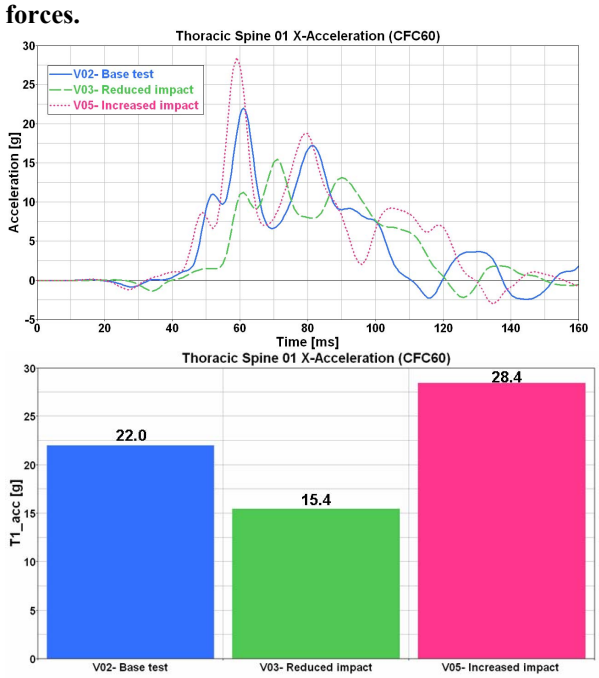

Figure 11. Effect of crash severity on T1 longitudinal acceleration.

Effect of Backset

Backset is the initial horizontal distance between the back of the dummy's head and the front of the head restraint. While the base test V02 featured a small backset, this distance was considerably increased in test V01, partially by changing the head restraint position relative to the seat back and by slightly modifiying the dummy posture. The initial positions are shown in Figure 12.

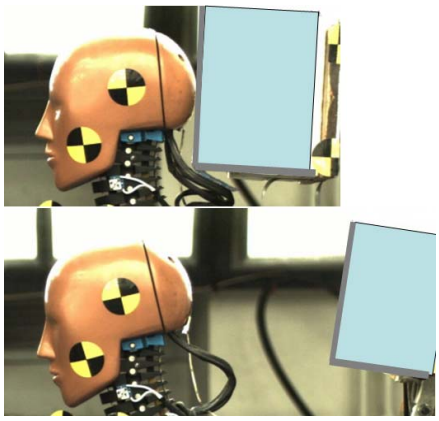

Figure 12. Initial dummy and head restraint position in test V02 (top) and V01 (bottom)

Changing the backset leads to large differences in neck loadings (see Figure 13). With increasing backset the tendency for positive shear in the neck, i.e., the head moving rearward in relation to the thorax, rises. The T1 acceleration was reduced in the test with larger backset, but the difference in dummy position probably contributed to this effect.

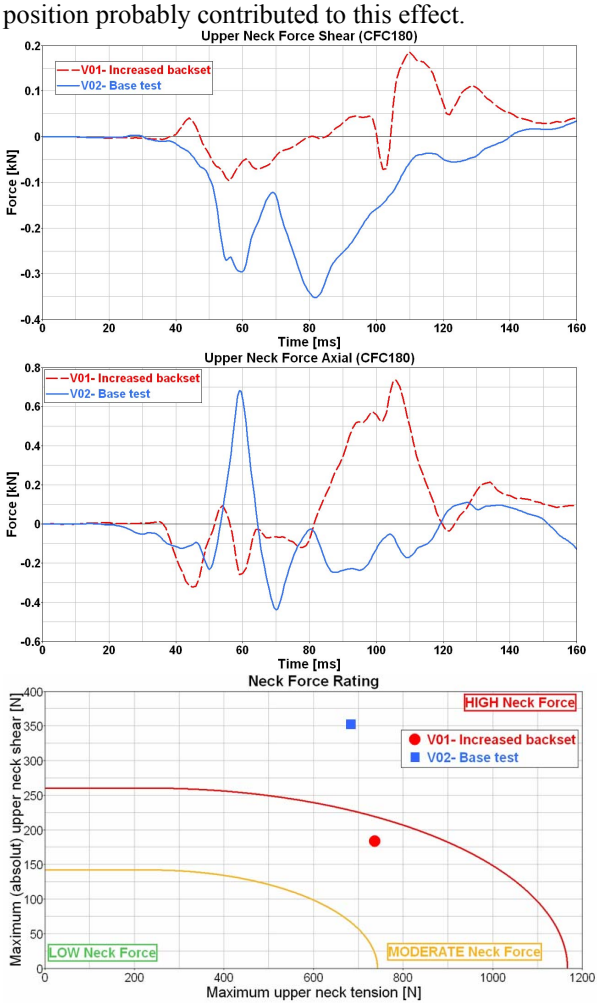

Figure 13. Effect of backset on upper neck forces.

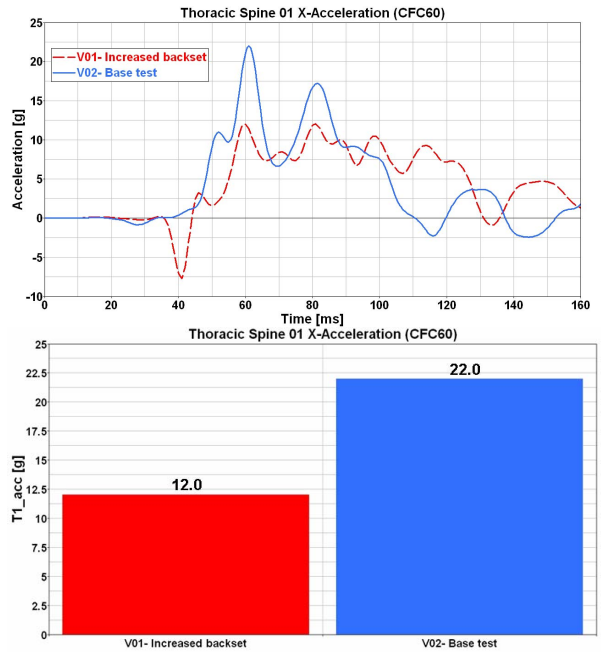

Figure 14. Effect of backset on T1 longitudinal accleration.

Effect of Seat Back Angle

When the seat back angle was increased in test V04 it was necessary to adjust also the dummy's posture. The initial situations for this and the base test V02 are compared in Figure 15.

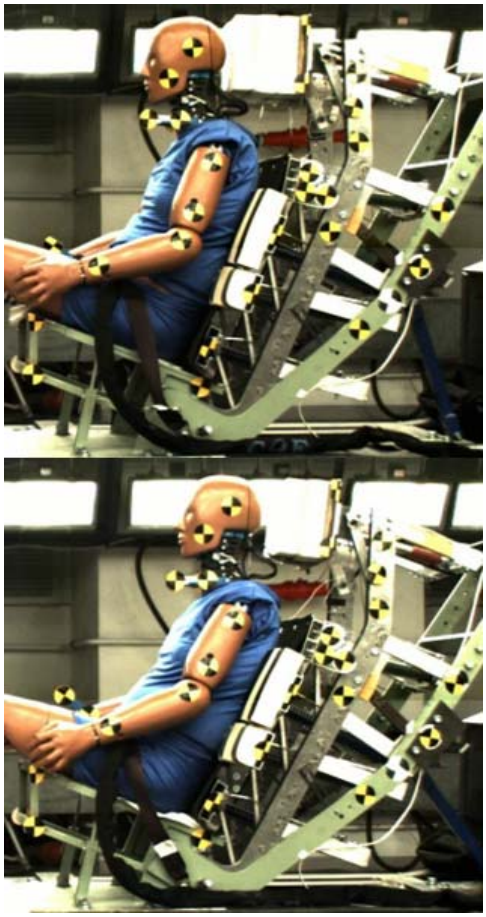

Figure 15. Initial dummy and seat position in test V02 (top) and V04 (bottom).

With stronger inclination of the seat back a reduction of the tension and shear force peak values as well as T1 acceleration can be observed. Nevertheless, this should not serve as a simple measure to reduce the biomechanical loadings in a rear-impact as it increases the risk of the occupant sliding over the seat back.

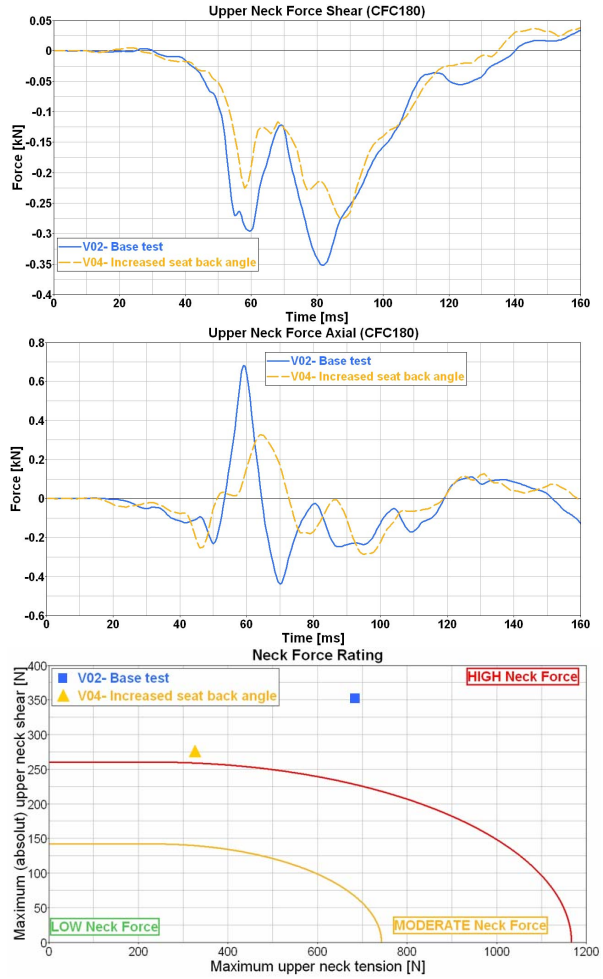

Figure 16. Effect of seat back angle on neck force.

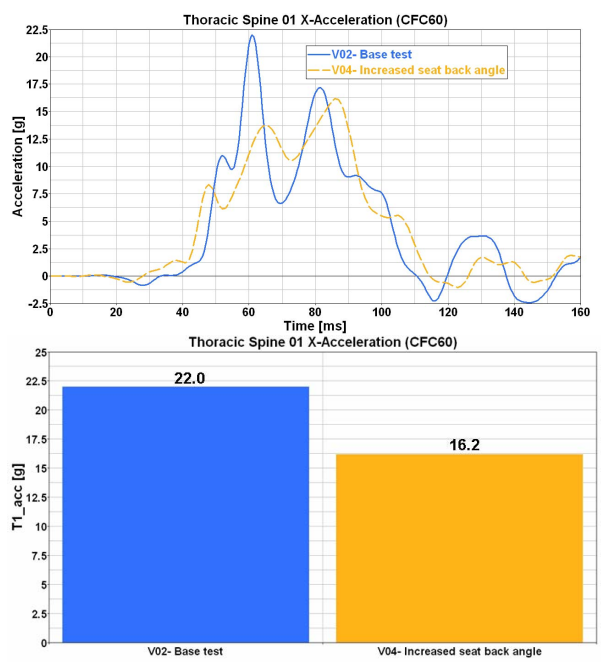

Figure 17. Effect of seat back angle on T1 accel.

Numerical Simulation Model

The simulation model was set up mostly as a multi-body model in MADYMO 6.3.2. The seat was built up completely new. For this purpose, the geometry of the Chalmers seat was digitized with a coordinate measuring device and modelled with the Pro/ENGINEER CAD software system. The mass inertias of inidividual seat parts were calculated on the basis of weight and geometry measurements. Spring characteristics were calculated based on the measurement of their specific geometries. The seat model was developed as a multi-body system with discrete masses and joints. In order to replicate the seat geometry as closely as possible the measured data were transferred into a facet model and superposed on the multi-body model.
A PAMCRASH finite element model was used to determine the characteristics of the sheet metal bending brake located between the seat back frame and the sub-frame since extensive experience regarding model set-up and material properties existed already. The obtained force-deformation characteristics were then transferred to the MADYMO model. The foam of the head restraint on the Chalmers seat was modelled in finite element code with solid elements.

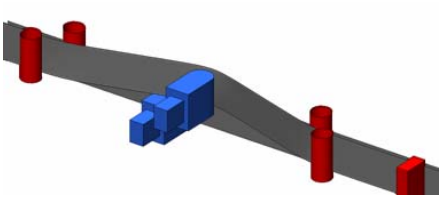

Figure 18. Numerical model of deformation element.

For the numerical representation of the BioRID II the current MADYMO dummy was used which includes facet surfaces (MADYMO 6.3.2, facet dummy version 2.1) (see Figure 19). The numerical model of the dummy was updated twice over the duration of the project. The initially employed model (MADYMO 6.2.2 with BioRID Version 1.1) showed geometric incompatibilities in the neck area due to an unrealistic representation of the geometry of the end stops which led to unnatural joint characteristics. The calculations were repeated when a BioRID II model update was available and provided a stable and satisfying result.

A sensitivity analysis was carried out to investigate the robusteness of the complete model which showed that the calculation requires a time step of one microsecond to avoid large numerical scatter in the results.

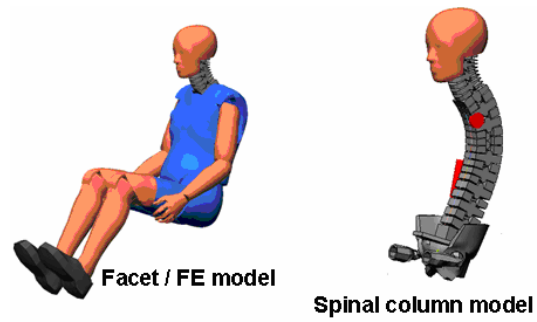

Figure 19. MADYMO BioRID II model.

VALIDATION OF SIMULATION MODEL

In a first step, the crash pulses measured in the validation tests were included in the MADYMO model. Dummy positioning coordinates from the basic test were processed in finite element code and superposed on the MADYMO model to allow accurate positioning of the numerical dummy model. H-point, legs and arms as well as characteristic points on the spine and head were positioned to coincide as much as possible with the measured pre-test dummy coordinates (see Figure 20). However, it proved difficult to adjust the model's spine in such a manner that the balanced position of the dummy model matched the initial seating posture of the real BioRID II dummy. When the numerical model was positioned accurately it produced high accelerations in the vertebrae when the calculation was started, yielding useless calculation results. Hence, the calculation was started with a relaxation phase of 50 milliseconds to eliminate the initial loading effect and allow the model to assume a balanced state. Any small movements of the dummy model during this relaxation were anticipated in the initial position so that the relaxed posture matched the seating position in the validation tests. Only then the complete model was subjected to the crash pulse and the actual simulation phase started. The positions of the joint coordinate systems were not adjusted as they can be expected to reflect the real geometry.

Figure 20. Positioning of dummy model.

The contacts between the dummy and the seating surface and the four seat back elements were defined such that only the characteristics of the dummy model were adapted; the seat surfaces were assumed to be undeformable. Because the foam in the hip area proved too soft an adjusted force-deflection characteristic was applied to produce a realistic behavior of this body region. The dummy could remain unchanged for proper definition of the contacts with the seat back elements. However, the choice of the friction model has considerable influence on the calculation result.
The foam used for the head restraint in the tests was relatively soft and required the use of a solid-foam model to reflect the non-linear effects of the geometry properly. Since no separate component tests could be conducted the foam properties were defined in the context of the complete simulation model.
A specific problem arises – at least in conjuction with the Chalmers seat design – from the fact that the facets of the dummy jacket are attached to the spine segments in the numerical model. In case of relative rotational movement between two adjacent spine segments the size of the facets on the back of the jacket changes. This effect can produce large deformations so that the jacket geometry becomes incorrect. This problem could be solved by adapting the contact characteristics.
The entire model was validated exclusively on the foundation of the base test V02. The validation quality of the numerical model can be judged by the comparison of both the kinematics and the major loading curves between numerical simulation and experiment. The motion of the dummy model matches that of the real dummy very well when their silhouettes are overlaid (see Figure 21).

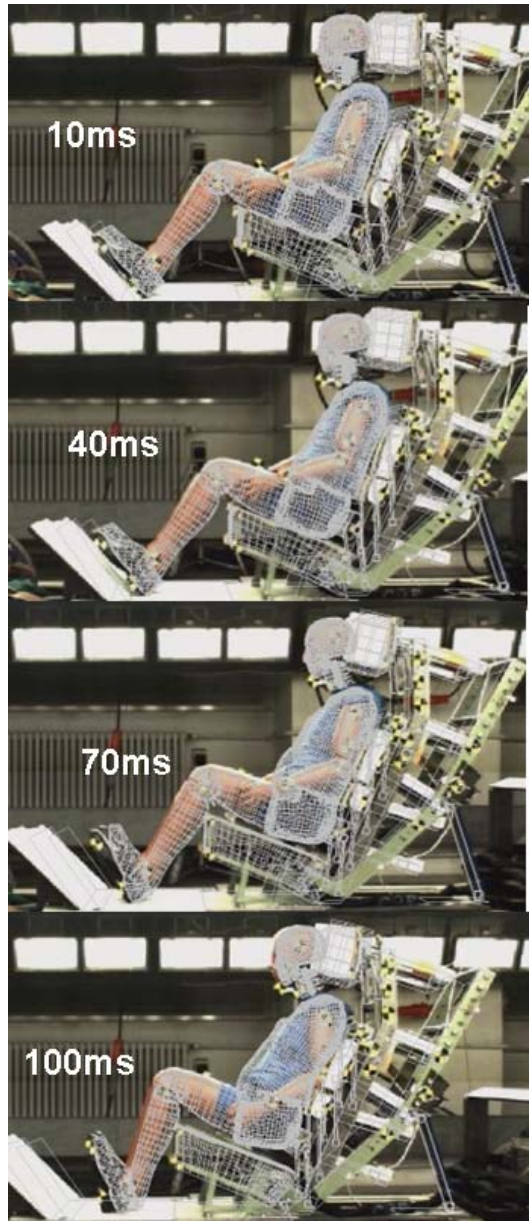

Figure 21. Comparison of kinematics in test and simulation for V02.

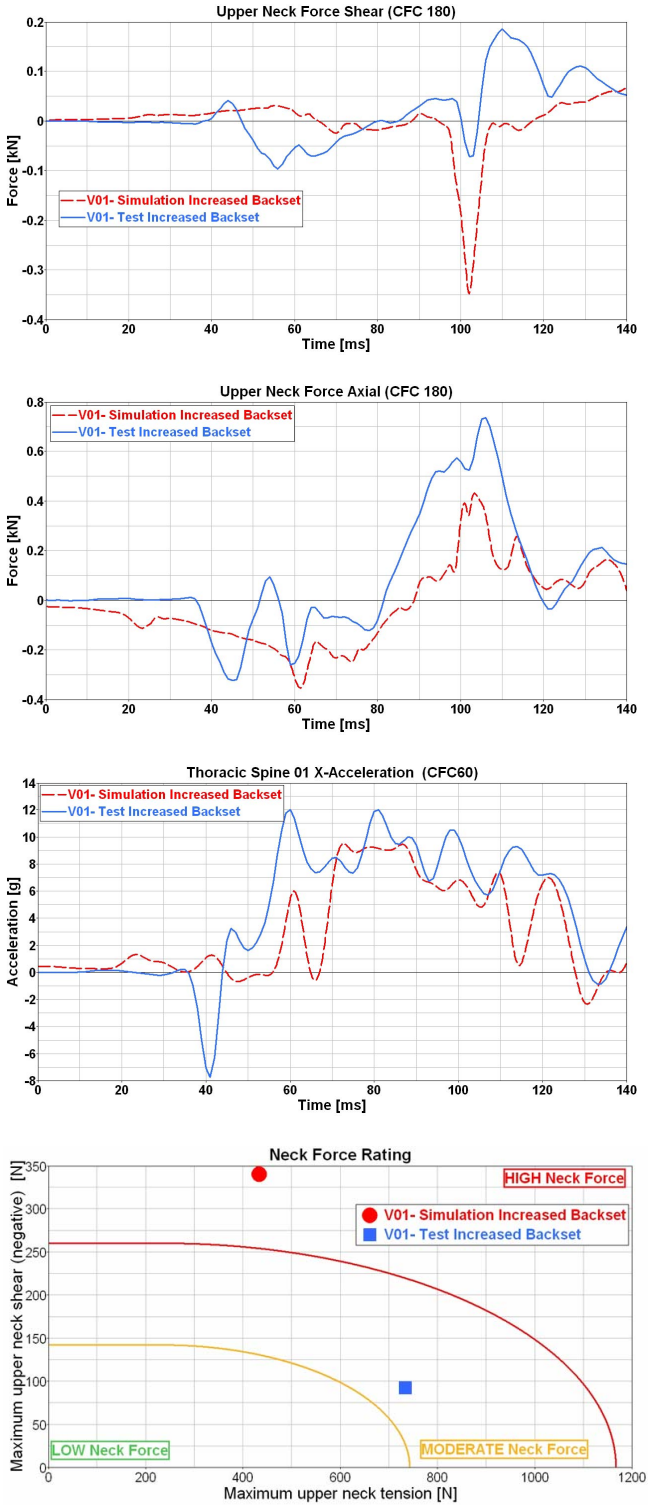

Figure 22. Validation result for test V01.

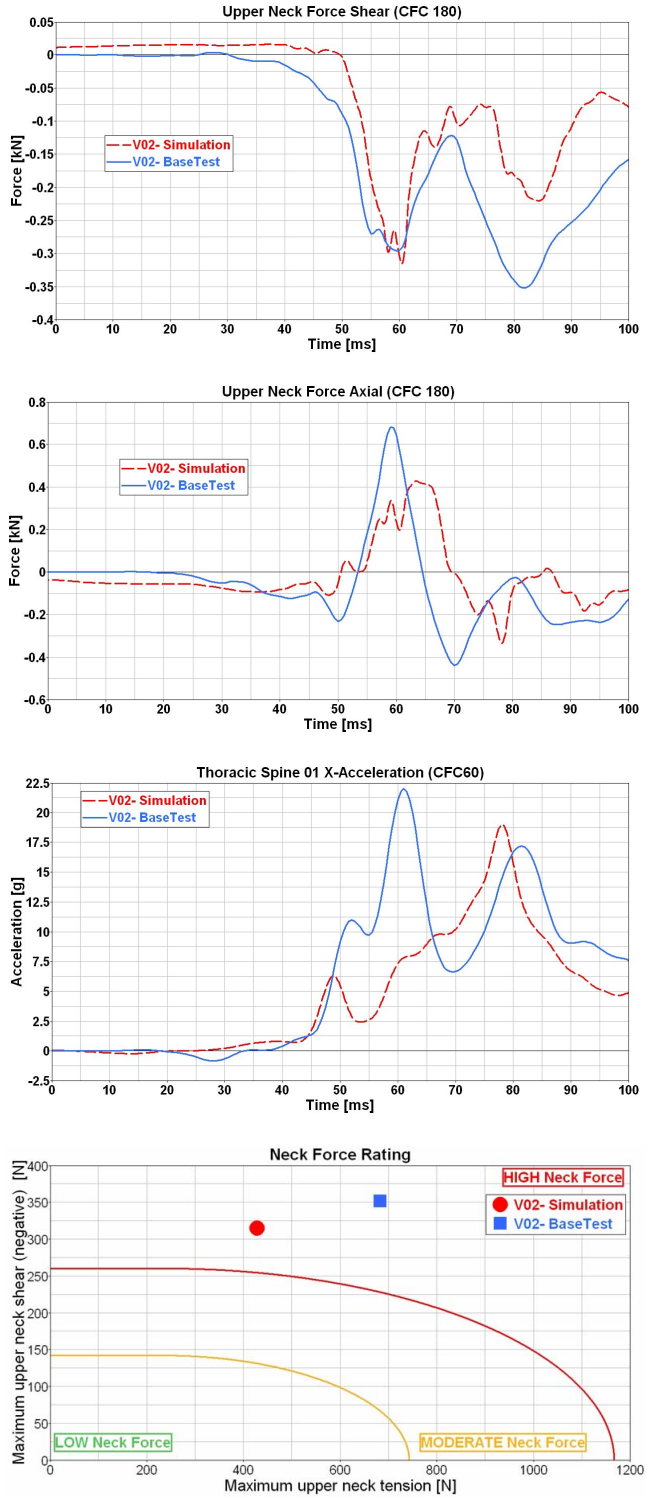

Figure 23. Validation result for test V02.

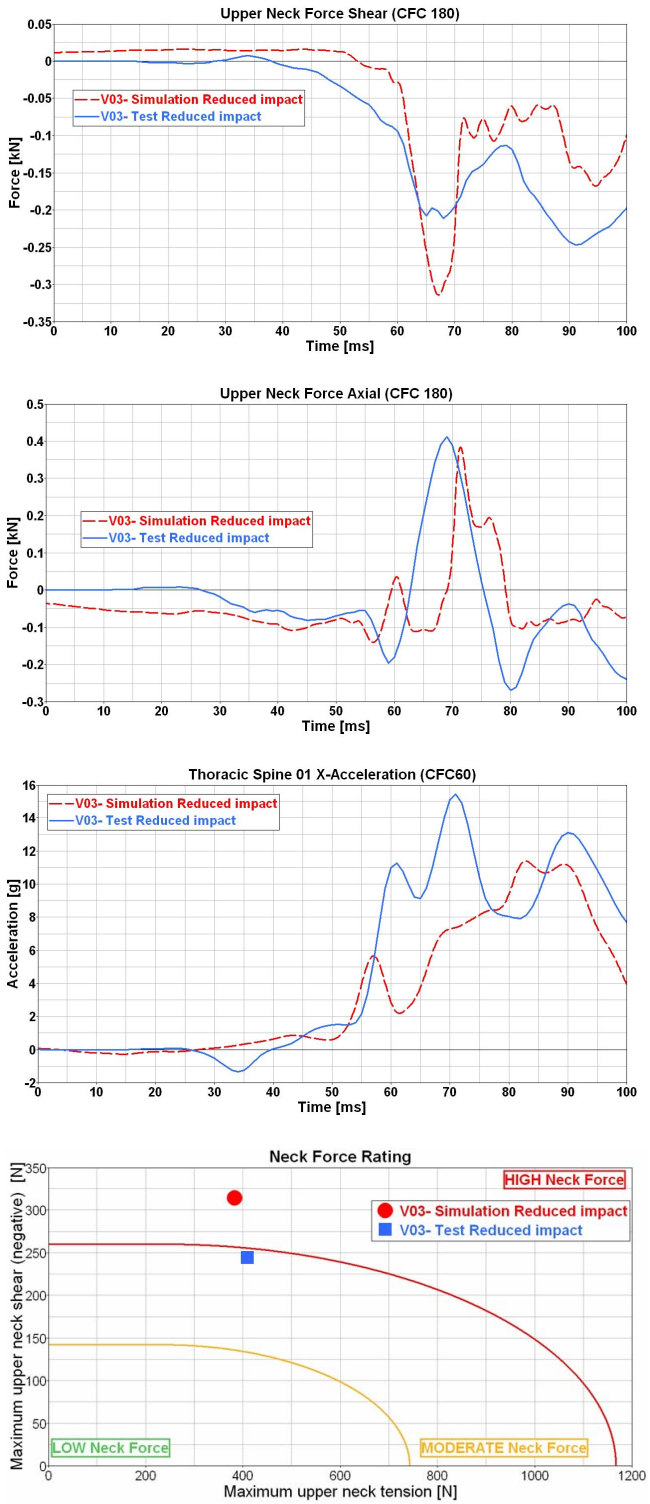

Figure 24. Validation result for test V03.

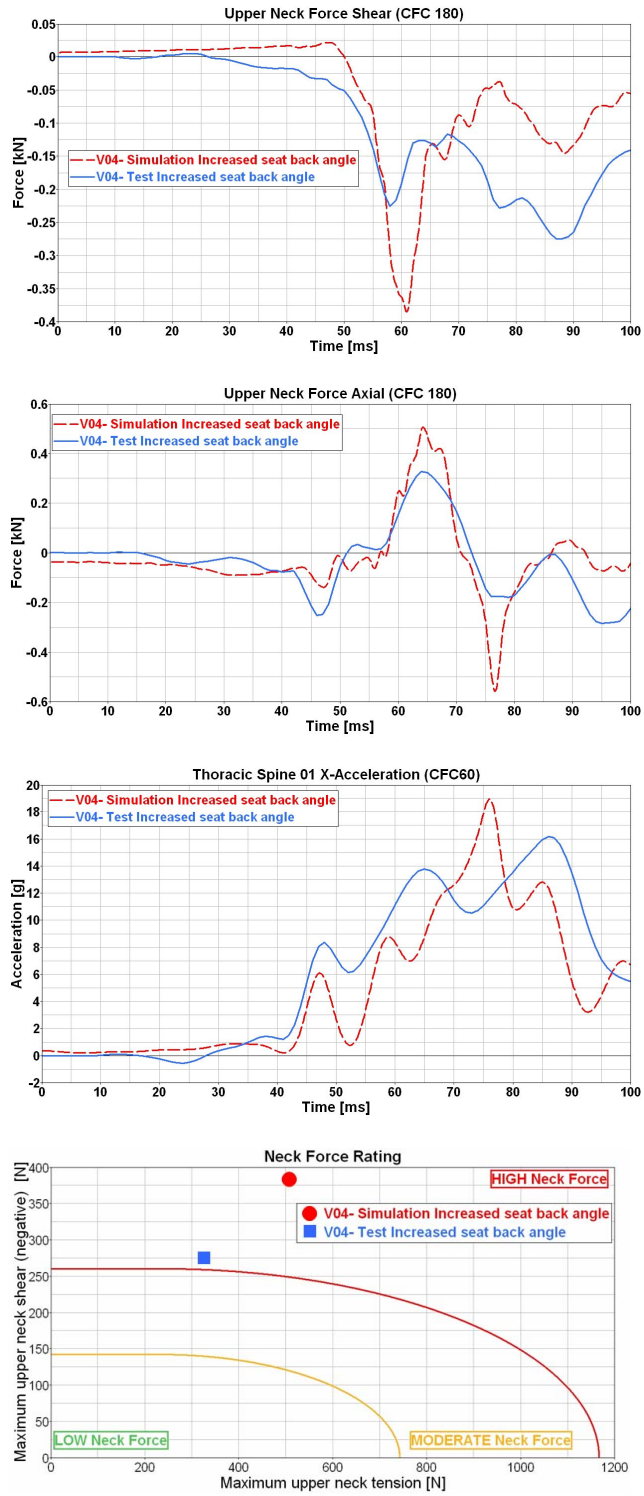

Figure 25. Validation result for test V04.

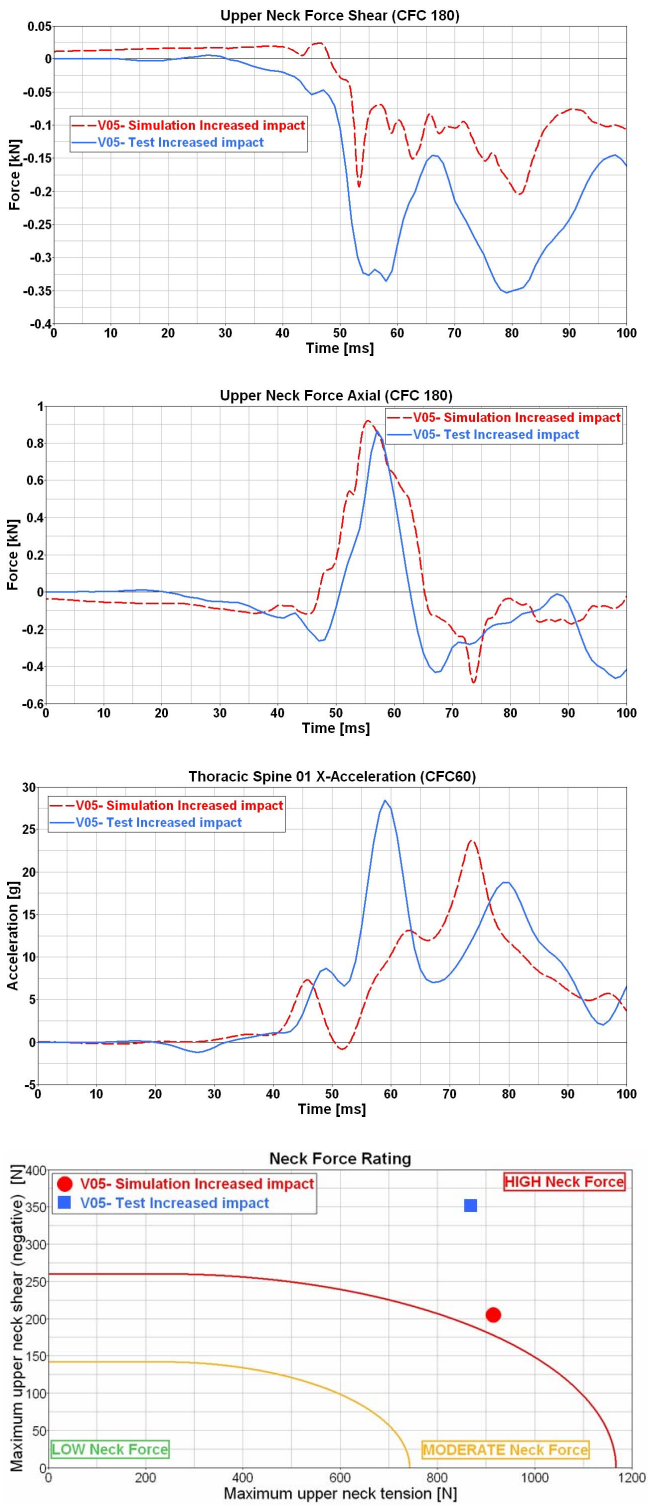

Figure 26. Validation result for test V05

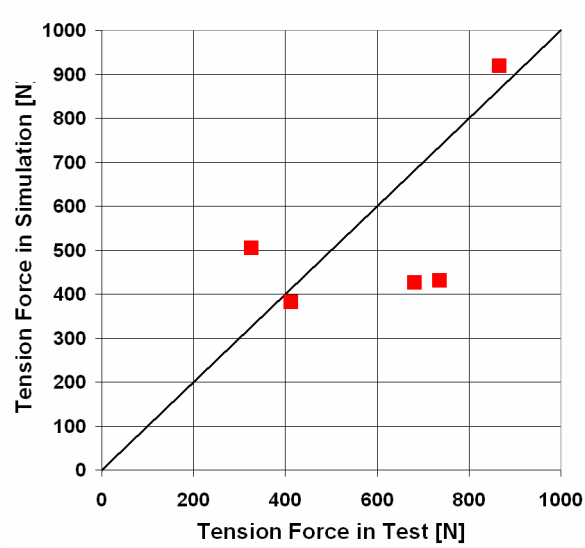

Figure 28. Upper neck shear forces.

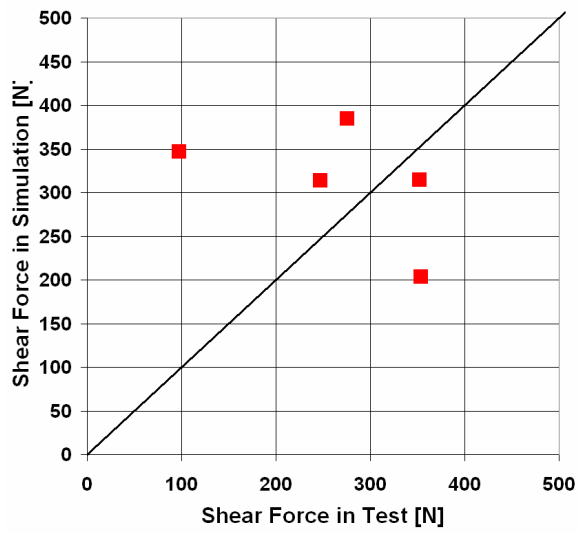

Figure 29. Upper neck tension forces.

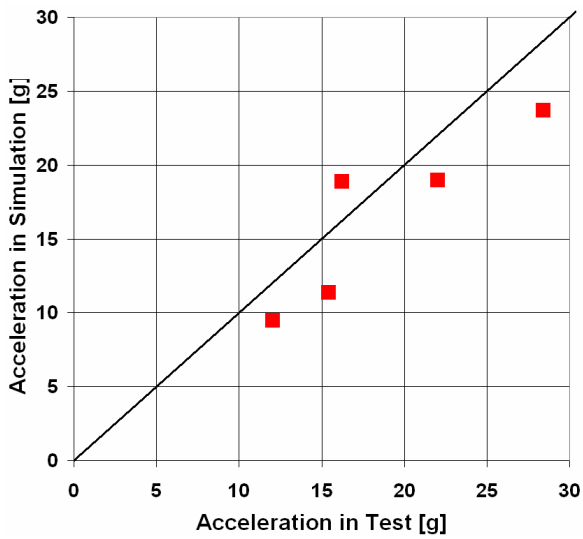

Figure 27. Thorax T1 accelerations.

	Upper Neck Shear Force	Upper Neck Tension Force	T1 Acceleration
V01	358%	59%	79%
V02	89%	63%	86%
V03	127%	93%	74%
V04	140%	155%	117%
V05	58%	106%	83%

Figure 30. IIWPG-relevant criteria from simulation in relation to test results (100%)

When comparing the characteristics of the dummy loading curves obtained from testing and calculated with the numerical model the criteria measured in the pelvic region corresponded well. The same holds true for the head accelerations. However, for the body regions which are relevant for IIWPG assessment the loading characteristics show less agreement. An overview of the extrema from the simulation model in relation to those measured in the tests is given in Figures 27 to 29 and Figure 30. Data from the rebound phase after the head contact with the head restraint had ended were not considered for this evaluation.

The IIWPG protocol assesses only positive shear force values and axial tension forces, i.e., a rearward relative motion of the head relative to the torso. The BioRID II dummy typically displays this behavior in rear-impact tests with production car seats. However, also negative shear forces occurred in some of the validation tests during the relevant phase of head-to-head restraint contact. This can be attributed to the particular configuration chosen for the Chalmers seat where the head restraint is closer to the head than usually found in production seats. Therefore and in contrast to IIWPG practice, the present study takes into consideration also negative shear values when illustrating simulation results in the rating chart and to assess the validation quality.

The axial forces are represented quite well by the simulation model, both in general character of the graph and in magnitude of the peak values, except for the test condition with increased backset V01 (see Figure 22 to 26). The peak values of the shear force differ significantly from those measured in the tests in some cases, but the times that the peaks occur correspond between simulation and experiment. This supports the visual ascertainment that the overall motion of the dummy model coincides with that of the test dummy. Again, the largest deviations between simulation and test curves are found in the situation with increased backset.

When analysing the longitudinal acceleration graphs of T1measurements most tests demonstrate a pronounced first peak at the beginning of the dummy loading phase. This peak is possibly caused when the head restraint accelerates the head and this signal is transferred through the cervical spine to the thorarcic spine. It is not prominent in the graphs obtained with the simulation model. Apart from this peculiarity, the T1 longitudinal accelerations are well represented by the numerical model in general character and in magnitude.

The complete simulation model which was validated only on the basis of test V02 predicts also the biomechanical loadings measured in test V03 (reduced crash severity) quite well. The conformity with the test results from V05 (increased seat back angle) and V06 (increased crash severity) is limited mostly due to the deviations in neck shear force. The test scenario which included a very large backset and modified initial dummy position (V01) is reflected only roughly in simulation although characteristic points in the kinematics between test dummy and model match.

DISCUSSION AND CONCLUSIONS

For the build-up of a numerical simulation model to study the influence of seat design factors on occupant loadings under rear-impact a number of validation tests were conducted. The chosen test set-up allows to adjust the crash pulse by means of a simple and cost-efficient method. Using a system which accelerates a stationary carriage with the seat and dummy enables to accurately measure the dummy position as it is present when the impact occurs. This is a pre-requisite for the subsequent simulation model validation. Five tests were conducted with the aim to cover a range of major influential factors on the occupant kinematics and biomechanical loadings. Accordingly, the crash severity and the seat geometry were varied in the tests. This allows to evaluate the

prognostic capabilites of the simulation model for a range of test conditions.
The generic seat design of the Chalmers seat employed in the dynamic experiments facilitates the adjustment of seat parameters independently of each other. The structure and geometry of this test device differs from those of many production car seats, e.g., in the area of the seat cushion and the connection between between seat back and head restraint. The dynamic behavior of the Chalmers seat may therefore deviate in detail from that of a production seat or at least require extensive pre-testing to adjust its characteristics. Particularly, it was found that the seat configuration used for some of the validation tests differed in behavior from most car front seats. The head restraint caught the dummy's head very early which resulted in uncommon neck shear force characteristics.
The tests provided input data to describe the experimental set-up in a numerical simulation model, mainly in multi-body code MADYMO. Particular elements of the seat model were realized in FE code and major surfaces which come in contact with the dummy model were carried out as facet surfaces to allow realistic interaction with the body parts. The model of the employed BioRID II anthropometric test device is based on multi-body code, but features a facet representation of the body surfaces. However, a considerable amount of validation work on certain body regions of the original dummy model was necessary to replicate adequately the interaction with the seat as observed in the experiments. The finite element version of the dummy model which was also available at the time of the study did not improve the simulation results significantly and was therefore abandoned. FE model updates that have entered the market in the meantime demonstrate more promising quality. Investigations of the model robustness revealed that the time step size for the calculation should not fall short of one microsecond. Future efforts to optimize the model should focus on improving the dummy model and its interaction with the seat surface. It is also possible that the difficulties encountered with the inconsistencies in the dummy back in conjuction with the Chalmers seat are less pronounced when production seats with a softer and continious seat back surface are used.
A recent MADYMO model version (MADYMO 6.3.2, facet dummy version 2.1) of the BioRID II with a water-filled abdominal cavity and jacket in FE method was implemented in the existing model. It indicates that the described difficulties in the dummy back region are largerly overcome, but would have required a completely new validation of the thoracic and cervical spine area. Hence, this approach was not further pursued in the course of the present study.
Another alternative is the utilization of a complete finite element representation of the BioRID II dummy which is also available on the market. Using the experience from the MADYMO-based simulation model it is planned to set up also a finite element version in LS-DYNA code. Future research in this field should therefore include a systematic evaluation of the different model approaches.
The calculated biomechanical loadings from the current simulation model correspond quite well with the characteristics of the measured accelerations and forces on the test dummy, especially for the head and the pelvic area. However, some significant deviations are evident in the neck and upper thoracic area which currently prohibit to use the model to forecast IIWPG-relevant loadings. Nevertheless, the model can be used to predict tendencies when seat design parameters or crash severity are varied. It can therefore be considered a suitable research tool to study the influence of fundamental rear-impact factors. However, it should be utilized only within the range of the tested conditions and should regard the limitations of the test set-up and the anthropometric test device. Possible subjects of application are the investigation of different crash pulse characteristics, seat back or head restraint positions on the biomechnical loadings of the BioRID II. A number of parameter variations with regards to the seat position has been conducted already which indicate positive effects on the seat performance.
The application of the model in a vehicle environment including a particular car seat could not be realized during this study. Provided that sufficiently detailed MADYMO seat models are available this offers possibilities for enhancing the safety of present or future seat concepts.

ACKNOWLEDGEMENTS

Appreciation is extended to the Loss Prevention Commission of the German motor insurers for funding the study and to Harald Morres and Samy Kassem for their leading contribution to the development of the test method and simulation model and conducting the experiments and analysis.
The authors would also like to thank Mats Svensson from Chalmers University, Sweden, and the Technical University of Graz, Austria, for making the Chalmers seat and BioRID II dummy available for testing.

REFERENCES

[1] Viano, D. C., Olsen, S. 2001."The Effectiveness of Active Head Restraints in Preventing Whiplash". Journal of Trauma, Vol. 51, pp 959-969

[2] Comité Européen des Assurances (CEA). 2004. "Minor cervical trauma claims". CEA/AREDOC – CERECOC

[3] International Insurance Whiplash Prevention Group. September 2006. "IIWPG Seat/Head restraint Evaluation Test Protocol", Version 2.4

[4] Farmer, C.M.; Wells, J.K.; Lund, A.K. 2003. "Effects of head restraint and seat redesign on neck injury risk in rear-end crashes". Traffic Injury Prevention Vol.4, pp 83-90

[5] EEVC WG20. March 2005. "Updated State-of-the-Art Review on Whiplash Injury Prevention", Working Document 80, pg. 6

[6] MADYMO Model Manual, Release 6.3.2, December 2006

EVALUATION OF THE 95TH PERCENTILE HIII LARGE MALE DUMMY

Joshua Shaw
Transportation Research Center Inc.
Edward Probst
Bruce Donnelly
NHTSA – VRTC
United States
Paper Number 07-0228

ABSTRACT

This study summarizes results from a preliminary evaluation of the Hybrid III Large Male Dummy. The paper reviews the dimensions, certification test responses, durability, and repeatability and reproducibility of two Hybrid III 95th Percentile Large Male dummies, each produced by a different manufacturer. Response data from multiple repeats of the proposed Calibration and Inspection Test Procedure sections from the SAE Draft of the "User's Manual for the HIII 95th Large Male Test Dummy" (SAE, 2003) are used as the basis for the analysis. An overview of the test methodologies employed is presented as well as an assessment of the compliance with the proposed certification specifications, durability at high energy test levels and repeatability and reproducibility. Besides employing the typical repeatability measures of traditionally-calculated coefficients of variation, a new technique is proposed and discussed involving a time-variant method of calculating coefficients of variation.

INTRODUCTION

The first anthropomorphic representation of a large male was developed by the Sierra Engineering Company in the late 1940's and early 1950's under contract to the U.S. Air Force. This 95th percentile anthropomorphic test device (ATD) known as "Sierra Sam," was primarily used for early aerospace and high altitude parachute experimentation. With the development of more biofidelic ATDs in the 1970's and early 1980's, such as GM's Hybrid generation of 50th percentile dummies, a foundation was established for the creation of a "family" of these advanced dummies.

In 1987 the Center for Disease Control (CDC) awarded a grant to the Ohio State University for the development of this Hybrid III (HIII) family of dummies. The SAE formed a task group of industry, government, and academic biomechanics experts to support this work through the generation of geometric and mass scale factors. These factors were applied to the HIII 50th percentile male specifications to develop dimensional, weight and impact performance requirements for 5th and 95th percentile HIII dummies.

Although the HIII 5th percentile small female is currently regulated by the Code of Federal Regulations, Title 49, Part 572, the 95th Percentile Large Male is not; albeit a 95th surrogate is referenced in FMVSS No. 202 governing head restraints.

The purpose of this evaluation is to support a future Federalization process by conducting a thorough inspection of component and full-dummy external dimensions of two HIII 95th large male dummies from different ATD suppliers. In addition, preliminary evaluations of the repeatability and reproducibility (R & R) and laboratory durability of each dummy are also performed.

Two draft documents currently being developed by the SAE Dummy Test and Evaluation Subcommittee are used as templates for the experimental aspects of this investigation. A draft version of the SAE Engineering Drawing Package (SAE EA 32) is used as the basis for a common dimensional and weight inspection of both dummies. The R & R test plan is based upon multiple repeats of the major certification tests enumerated in the SAE draft of the "Users Manual for the HIII 95th Large Male Test Dummy" (SAE, 2003). The durability assessment is developed by scaling the certification tests to energy levels associated with proposed injury levels for the large male.

For the purposes of this project two dummies were purchased from two manufacturers, one from Denton ATD (DATD) and one from First Technology Safety Systems (FTSS). Dummy #077 is from DATD and dummy #226 is from FTSS.

METHODS

Inspection

The drawing review process involves examining all of the engineering drawings for clarity and accuracy. These drawings are checked both by comparing the physical part dimensions to the drawing dimensions as well as by comparison to the contents of other federally regulated dummies, such as the HIII 50th percentile male dummy. The inspection process is a

physical check of the dummy components in both segment weights and external dimensions. This can also include the inspection of individual part dimensions to the corresponding drawing(s). The segment weights and external dimensions of each dummy are listed in the Results section along with the specification.

Certification Testing

The certification tests utilized to determine the repeatability and reproducibility of the HIII 95th Large Male dummy are those as specified in the SAE User's Manual. These types of tests are the same as those specified for the 50th percentile Hybrid III dummy, but the dynamic response requirements have been scaled (Mertz, 1989) for a large male dummy based on geometric similitude. The tests specified by the User's Manual include frontal thorax impact, frontal neck flexion and extension tests, knee impact, and knee slider impact.

Head Drop Certification Test - Head drop certification tests are conducted by dropping an isolated head from a height of 376 mm onto a 50.8 mm thick steel plate and measuring the triaxial acceleration at the center of gravity (CG) of the head. The resultant acceleration is calculated from the filtered acceleration time histories and according to the SAE User's Manual should be between 220 – 265 g at peak and the lateral acceleration (Y axis) should be less than 15 g in either direction (positive or negative Y axis). Mertz et. al. (1989) specifies the same acceleration range for the head drop.

Neck Flexion Certification Test - The neck flexion and extension tests are conducted using a pendulum to which the neck and head are attached. The pendulum is released from a given height to produce a desired velocity at the bottom of the swing arc. As it reaches the bottom vertical position it is arrested by an energy absorbing component. Although the pendulum arm motion stops, the inertia of the head causes the neck to flex in relation to the pendulum. A six axis upper neck load cell was used to record the forces and moments generated about the occipital condyle (OC) joint while two rotary potentiometers and a connecting rod are used to determine the angle of the head in relation to the pendulum, which represents the torso. This angle is known as D-plane rotation.

The SAE User's Manual specifies an impact velocity of 6.89 – 7.13 m/s at the pendulum CG and a pulse profile measured by the integrated pendulum acceleration, to define the energy absorbing component. Mertz et. al. (1989) also specifies a corridor for the neck flexion response. The corridor coordinates are shown in Table 1.

Table 1.
Mertz et. al. OC moment versus D-plane angle neck flexion corridor

Upper Boundary Coordinates		Lower Boundary Coordinates	
Moment [Nm]	Rotation [deg]	Moment [Nm]	Rotation [deg]
0	0	0	34
83	14	37	53
83	43	120	73
120	64	258	77
258	68		

Neck Extension Certification Test - The SAE User's Manual specifies an impact velocity of 5.90 – 6.19 m/s at the pendulum CG and a pulse profile as measured by the integrated pendulum acceleration. Mertz et. al. (1989) also specifies a corridor for the neck extension response. The corridor coordinates are shown in Table 2.

Table 2.
Mertz et. al. OC moment versus D-plane angle neck extension corridor

Upper Boundary Coordinates		Lower Boundary Coordinates	
Moment [Nm]	Rotation [deg]	Moment [Nm]	Rotation [deg]
0	0	0	-48
-42	-19	-11	-77
-42	-58	-92	-92
-65	-77		
-92	-82		

Thorax Certification Test - The thorax certification test is a frontal impact to the dummy chest centered midsternally with a 23.36 kg pendulum traveling at a velocity of 6.71 +/- 0.12 m/s at impact. In addition to the peak response requirements stated in the SAE User's Manual, Mertz et. al. specify a force versus deflection corridor (Table 3) for the entire impact.

Knee Impact Certification Test - Knee impacts are administered at velocities between 2.07 – 2.13 m/s by a 5-kg pendulum to the knee of a flexed lower extremity. It was assumed that both knees of the same dummy are the same and therefore only one knee from each dummy is compared.

Table 3.
Mertz et. al. force versus deflection thorax corridor

Upper Boundary Coordinates		Lower Boundary Coordinates	
Force [kN]	Deflection [mm]	Force [kN]	Deflection [mm]
4.85	6.6	3.65	6.6
5.07	26.4	3.78	2.64
5.34	39.6	3.96	3.96
6.05	64.8	4.45	6.07
4.94	80.8	3.47	6.35
3.47	85.9	0.98	5.41
0.98	76.7		

Knee Slider Certification Test - The knee slider certification test was conducted in nearly the same manner as the knee impact test. However, the lower portion of the leg is removed and an impact fixture is attached to the knee slider. A 12-kg pendulum strikes the fixture at velocities between 2.70 – 2.80 m/s. Rather than the SAE specified deflection response, Mertz et. al. specified a stiffness corridor, 137 – 187 N/mm.

Repeatability and Reproducibility

In the traditional method for assessing the repeatability and reproducibility of a dummy design, a test is repeated a number of times and the average, standard deviation, and coefficient of variation (CV) of the peak of the response parameters are quantified. Accepted practice is that a CV between 0 – 5% is Excellent, 5 – 8% is Good, 8 – 10% is Acceptable, and > 10% is Unacceptable (Rhule 2005). Once a dummy response is shown to be repeatable (by displaying an acceptable or better CV), the reproducibility is assessed by combining the results from all tests of all dummies and applying the same standard for CV. This approach has several shortcomings and a modified approach will be followed in this study.

The traditional approach for assessing dummy repeatability, as described above, has been to test a dummy several times, in identical configurations, and to calculate the CV at the maximum points of a relevant response parameter. This approach assesses the dummy response at the point in time at which most certification criteria are established, e.g., maximum chest force or maximum neck rotation. The drawback to this approach is that the dummy response is a time history and the time at which the maximum value occurs, as well as the overall shape of the response, is important. When comparing maximum response values from repeat tests the values may not be occurring at the same point in time and a small or large CV may not actually be a valid assessment of repeatability. Further, it may be that the maximum values are the only point in time at which the dummy responses are similar and the repeatability is actually poor at all other points in time. In this study of the 95th percentile male dummy an assessment of repeatability will be made over a portion of the response time history.

A set of six force versus time response curves from the thorax certification tests conducted on dummy 077 are shown in Figure 1.

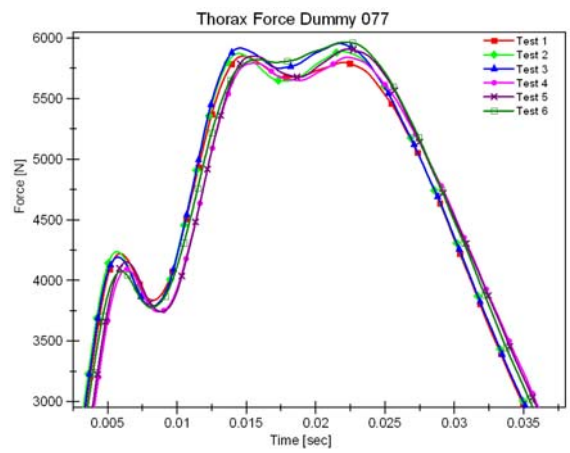

Figure 1. Central portion of force versus time response for certification tests conducted on dummy 077.

It can be seen that the curves are all quite similar but that there are slight differences in magnitude and timing of peaks, e.g., Test 1 curve versus Test 2 curve. A mean force versus time curve can be generated from these six digitized curves by averaging the force values at each time increment. Similarly, a standard deviation and a coefficient of variation for the six responses can also be generated at each time increment. At the maximum mean force (0.0221 seconds) the CV is 1.1%; however, at another point in time near the maximum mean force (0.0157 seconds) the CV is 0.5%; less than half. For the portion of the curve that is above half of the maximum value (i.e., all data above 50% of the peak value of the mean curve), the central portion of the response data, the CV varies from 0.5% to 8.5% with an average CV of 2.2%. Although the majority of these CV values are below the accepted standard of 5%, indicating very good repeatability, the CV calculated in the traditional manner (1.1%, see Table

13) is not representative of the CVs over the central portion of the curve.

If it is assumed that the important part of a response curve is the central portion of the curve, a confidence interval band can be drawn around the mean based on the sample response curves obtained from the six tests. It can be stated that we are 90% confident that the true mean lies within a confidence interval estimated from the sample responses we have. The equation for calculating a confidence interval (CI) is (Bendat, 2000):

$$CI = \mu \pm \frac{S(t_{\alpha/2})}{\sqrt{N}} \tag{1}$$

where S = the unbiased sample standard deviation as a function of time
μ = the sample mean value as a function of time
N = the number of tests
$t_{\alpha/2}$ = the two-tailed t-statistic for 90% = 2.015.

Thus, the confidence interval band (CI_B) (the projected range of mean variation about the sample mean) can be defined as:

$$CI_B = 2 * \frac{S(t_{\alpha/2})}{\sqrt{N}} \tag{2}$$

In can be stated that one half of the confidence interval band divided by the sample mean is analogous to the CV

$$\frac{CI_B}{2\mu} = \frac{S(t_{\alpha/2})}{\mu\sqrt{N}} = \frac{CV(t_{\alpha/2})}{\sqrt{N}} \tag{3}$$

Note that the unbiased standard deviation divided has a denominator of N-1 whereas the biased standard deviation, with a denominator of N, is normally used in the traditional CV calculation ([N/(N-1)]=1.09 times the biased CV yields the unbiased CV for N=6). If the "excellent" value of CV=5% is used in the calculation, the 90% confidence interval is ±4.5% of the sample mean, as shown below.

$$\begin{aligned} \frac{CI_B}{2} &= \frac{1.09CV(t_{\alpha/2})}{\sqrt{N}} \\ &= \frac{1.09(0.05)(2.015)\mu}{\sqrt{6}} = 0.045\mu \end{aligned} \tag{4}$$

In other words, if the sample response data has a CV of 5%, we can be 90% confident that the true mean lies within a ±5% corridor (actually 4.5%) of the mean. Practically speaking, it is 90% certain that the calculated mean is a good estimate of the true response. Similarly, if the sample response data has a CV of 10%, we can be 90% confident that the true mean lies within a ±10% corridor (actually 9%) of the mean. This analysis makes the usual assumptions of statistical independence and a normal distribution of response data. It must be noted that the number of repeat tests in this example was limited by practical considerations to N=6.

In this study repeatability will be assessed by calculating the CV at all points in the time history of the central portion and averaging all of these values to obtain a representative CV for that portion. If the average CV is below 5% the repeatability will be considered to be excellent.

Dummy to dummy reproducibility, where each dummy has already been shown to be repeatable, is assessed with a comparison of means by the Student t-test. A null hypothesis is selected stating that the average of the absolute value of the paired differences between the two dummy means is greater than 10% of the mean of the means. We will test this hypothesis using the one-tailed T statistic tested against the Student t-value at the 10% probability level (α = 0.05). The degrees of freedom will be the number of pairs, which is large and can be considered as infinity when using the table of t-values. The test statistic uses the standard error for the paired differences.

$$T = \frac{\sum_{i=1}^{d} \left[(0.1)(\mu_i) - |\mu_{1i} - \mu_{2i}|\right]}{(S_d)(\sqrt{d})} \tag{5}$$

Where μ_1 and μ_2 are the sample means
μ = the mean of the means
d = the number of pairs of data points
S_d = the standard deviation of the differences.

If the test statistic is larger than the t-value of 1.282 the null hypothesis is rejected and we can assume the responses from the two dummies are from the same population and can be combined. If the two sets of data are likely from the same population, it is reasonable to calculate a mean from all of the data for the dummy and apply the same procedure as was discussed previously for repeatability. In the case of reproducibility we will apply the more liberal 10% standard of acceptable reproducibility. If the two dummies are significantly different, i.e., if the null

hypothesis is not rejected, then the dummies are not reproducible.

Durability

To determine the durability of a dummy component, the input is incrementally increased to levels above the standard certification tests and the component inspected between test intervals. All dummies are designed and created with the intention of being used in a situation that could potentially cause injury to a human. Dummies are routinely subjected to events at or near the injury level in actual crash testing. Therefore it is necessary to have a dummy that is durable up to and beyond the injury levels that have been identified.

Injury levels for the 95th Male dummy were either determined from the corridors in Mertz (1989) or by scaling the injury values for the Hybrid III 50th Male listed in 49 CFR 571.208 up to the 95th Male using the scale factors listed in Mertz. It should be noted that the values employed are <u>not</u> the Injury Assessment Reference Values that would accompany a Final Rule for the 95th percentile dummy. Rather they are simply values used to determine an upper level that the durability testing should attempt to reach. The injury values that were determined to be sufficient for this testing are listed in Table 4.

Table 4.
Assumed injury levels for 95th Male dummy

Body Segment	50th Male Injury Level	95th Male Injury Level	95th Value Source
Head	HIC_{36} 1000	HIC_{36} 1000	49 CFR 571.208
Neck Flexion	OC Moment 190 Nm	OC Moment 258 Nm	Assumed Mertz (1989)
	$\Theta = 80°$	$\Theta = 77°$	Assumed Mertz (1989)
Neck Extension	OC Moment 57 Nm	OC Moment 92 Nm	Assumed Mertz (1989)
	$\Theta = 95°$	$\Theta = 92°$	Assumed Mertz (1989)
Thorax	Deflection = 76 mm	Deflection = 79 mm	49 CFR 571.208
	Force = 5.43 kN	Force = 6.05 kN	49 CFR 571.208
Knee	Force = 10 kN	Force = 12.7 kN	49 CFR 571.208

The data from Table 4 was then used to determine the inputs for durability testing. Rhule et. al. (2005) simply increased the input energy by a nominal 30%. Doing this however did not guarantee that a test type would result in a response at or exceeding the injury values. For the current study the outputs were used in a variety of engineering relations to determine the inputs required to produce a desired response. For example, to achieve the thorax injury level of a force of 6.05 kN and a deflection of 79 mm, the 23.4 kg pendulum mass must impact the dummy chest at some as-yet-unknown velocity. Conducting an energy balance calculation that relates the work done to the input energy, the input velocity can be determined. The specific approach for each test type is described below.

<u>Head Drop</u> - The Head Injury Criteria (HIC_{36}) is specified at 1000 for both the 5th percentile small female and the 50th percentile male dummies (49 CFR 571.208), therefore there was no reason to change the injury level for the larger 95th percentile dummy. HIC_{36} was calculated for several of the certification tests completed prior and it was noted that the values obtained were nearly at 1000. As a result the maximum head drop distance was increased to the greatest height that the in-house drop fixture would allow to achieve HIC_{36} results above 1000. The head was then dropped from the standard certification test height (376 mm), an intermediate height (415 mm), and the highest height (450 mm).

<u>Neck Flexion</u> - Injury values for neck flexion were derived from the corridors specified in Mertz (1989). The angle and moment were then used in an energy calculation to determine the input kinetic energy and thus the input pendulum velocity. It was assumed that the input translational kinetic energy would be converted to the output rotational work in this test type. Before the injury level velocity was determined a nominal loss term was calculated from the certification test averages so that losses could be approximated in the higher energy tests. For example, the average input velocity was 6.99 m/s and the average moment and rotation were 125 Nm and 61°, respectively. Solving the energy equation for the loss portion gives

$$Loss = \frac{1}{2}mv^2 - M\theta \qquad (6)$$

where m is the mass of the head and neck (6.65 kg), M is the moment, and θ the rotation,

$$Loss = \frac{1}{2}6.65kg * \left(6.99\frac{m}{s}\right)^2 - 125Nm * 1.06radians \quad (7)$$

which equals a loss of 30.1 joules. Now if Equation 6 is algebraically manipulated to solve for velocity and the injury level values and the loss term are input, it becomes

$$v = \sqrt{\frac{2}{m}\left(M\theta + Loss\right)} \quad (8)$$

$$v = \sqrt{\frac{2}{6.65kg}\left(258Nm * 1.34rad + 30.1J\right)} \quad (9)$$

The velocity required to produce the injury level is 10.6 m/s. Therefore the neck flexion tests would be performed at the certification test velocity (6.99 m/s), at an intermediate level (8.80 m/s), and at the injury producing level (10.6 m/s). Unfortunately, the equipment available could only reach heights capable of producing a 7.50 m/s impact velocity. It was decided to test at the certification velocity (6.99 m/s), an intermediate velocity (7.25 m/s), and the upper limit of the equipment (7.50 m/s).

Neck Extension - The same activity was completed for the neck extension test to determine the input required to produce an injury event in the dummy. The injury values for extension were also assumed from the corridors specified in Mertz (1989). Equation 6 was used again to determine the nominal loss in a standard neck extension certification test. The average velocity for these tests was 5.99 m/s and the average moment and rotation were 67.4 Nm and 79.0°, respectively. Solving Equation 6 with these inputs gives,

$$Loss = \frac{1}{2}6.65kg * \left(5.99\frac{m}{s}\right)^2 - 67.4Nm * 1.38radians \quad (10)$$

where the loss equals 26.3 joules. Similar to the neck flexion test, the injury level inputs and the loss term are used in Equation 8 to determine the velocity that would cause an injury reading

$$v = \sqrt{\frac{2}{6.65kg}\left(92Nm * 1.61rad + 26.3J\right)} \quad (11)$$

the required velocity was 7.24 m/s. This velocity was attainable and the dummy necks were tested at the certification velocity (5.99 m/s), an intermediate level (6.60 m/s), and the injury level (7.24 m/s).

Thorax - The determination of the input energy for the thorax impact test to achieve injury level was similar to that of the neck flexion and extension. For this test however, the input kinetic energy was related to the linear work output. Also similar was the calculation of the nominal energy loss in the certification tests. Using the average impact velocity, peak force, and peak deflection, the loss was calculated as follows

$$Loss = \frac{1}{2}mv^2 - Fd \quad (12)$$

where m = 23.36 kg and v, F, and d are the averages from Table 10 to give

$$Loss = \frac{1}{2}23.36kg * \left(6.75\frac{m}{s}\right)^2 - 5.79kN * 67.7mm \quad (13)$$

which results in a nominal loss of 140 joules. Equation 12 is algebraically manipulated to solve for velocity

$$v = \sqrt{\frac{2}{m}\left(Fd + Loss\right)} \quad (14)$$

and the injury level parameters are used to determine the velocity required

$$v = \sqrt{\frac{2}{23.36kg}\left(6.05kN * 79mm + 140J\right)} \quad (15)$$

which is 7.27 m/s. The in-house equipment had the ability to conduct impacts at greater speeds and therefore it was decided to test at the maximum velocity the equipment could produce. The thoraces of the dummies were tested at the certification velocity (6.75 m/s), an intermediate velocity (7.50 m/s) which is near the injury level, and at the highest velocity attainable (8.33 m/s).

Knee Impact - The knee impact test does not measure a deflection, but rather just a force. Instead of balancing the energy to determine the injury level input, the velocity requirement was found using conservation of linear momentum

$$mv_f - mv_i = \int Fdt + Loss \quad (16)$$

where m is the mass of the pendulum and v_f is approximately 0.73 m/s in the opposite direction after the impact. The loss was accounted for in the standard certification test as follows

$$Loss = m(v_f - v_i) - \int Fdt \tag{17}$$

$$Loss = 5kg\left(-0.73\frac{m}{s} - 2.10\frac{m}{s}\right) - .5(.00475s)(-6451N) \tag{18}$$

and found to be 1.98 kgm/s. The impulse was approximated by integrating a triangular waveform with a height equivalent to the average peak force and a base equivalent to the duration of the force pulse from the certification tests. Now solving Equation 16 for v_i to obtain the injury level output gives

$$mv_i = mv_f - \int Fdt - Loss \tag{19}$$

with the final, or rebound, velocity being a product of the input velocity. Therefore, the coefficient of restitution, 'e', was calculated from the certification parameters such that

$$e = \frac{mv_f}{mv_i} = \frac{0.73\, m/s}{2.10\, m/s} = 0.35 \tag{20}$$

which makes Equation 19 become

$$mv_i - mev_i = -\int Fdt - Loss \tag{21}$$

$$v_i = \frac{-\int Fdt - Loss}{m(1-e)} \tag{22}$$

Substituting the calculated loss, the desired force value and the mass into this equation allows for the determination of the velocity required to produce the injury level force response. The duration of the force response was assumed to be equivalent to that of the certification tests. Thus

$$v_i = \frac{-.5 * .00475s * (-12700N) - 1.17kgm/s}{5kg(1-0.35)} \tag{23}$$

results in a velocity of 8.89 m/s. This velocity is greater than the highest velocities attainable on the knee impact fixture. Therefore the equation was solved using a different mass, indicating a different pendulum to be used. The decision was made to use the 12 kg pendulum that was specified for the knee slider tests, rather than the standard 5 kg impactor, to reduce the required velocity. Solving Equation 23 again with a higher mass results in a velocity of 3.70 m/s, a value much more reasonably attained. Since the test velocity was to be incrementally increased from the certification velocity, it was decided to use the larger mass for all of the durability impacts rather than switching part of the way through the test plan.

Therefore, the certification test velocity would have to be reduced to account for the larger mass. The velocity was scaled based on kinetic energy from the 5 kg, 2.10 m/s impact to the 12 kg impact. This resulted in a 1.36 m/s impact required to maintain the input kinetic energy requirement. The knee impact test velocity was incremented up to the injury level similar to the other tests. The adjusted certification test velocity was completed first (1.36 m/s), then an intermediate velocity (2.53 m/s), and then the velocity required to produce injury (3.70 m/s).

RESULTS

Inspection

The inspection of each dummy yielded a positive result. The weights for all segments of both dummies were within the specifications. The majority of the external dimensions were within the specification for both dummies, however the 'hip pivot from backline' and the 'head circumference' were outside of the specification on dummy 226. The 'reference location for chest circumference' was also slightly high for both dummies. The measurements for both dummies can be seen in Tables 5 and 6 and Figure 2.

Certification Testing

Head Drop Test – The results for the head drop certification test are listed in Table 7 and the response time histories are shown in Figures 3 and 4 along with the SAE and Mertz corridors. The head resultants for dummy 226 were at the top bound of the corridor while the resultants for dummy 077 were just slightly higher than the top bound of the corridor. Dummy 226 had essentially no differences in phase while dummy 077 had slight differences. Both dummies had nearly the same duration for the impacts.

Neck Flexion – The results for the neck flexion certification test are listed in Table 8 and the response time histories are shown in Figures 5 and 6 along

with the SAE and Mertz corridors. The neck flexion responses were similar for each dummy but were just short of the corridor. Dummy 077 had three of the six tests enter the corridor but dummy 226 only had one test enter the corridor. Dummy 226 only obtained one value for the OC Moment within the rotation interval and, as a result, an average, standard deviation, and CV could not be calculated. Subsequently a CV could not be calculated for reproducibility for this parameter. All of the tests on both dummies did however match the Mertz corridor fairly well, with the peak portion being the exception.

Neck Extension – The results for the neck extension certification test are listed in Table 9 and the response time histories are shown in Figures 7 and 8 along with the SAE and Mertz corridors. The neck extension responses were quite similar but again were just short of being within the corridor. None of the tests for either dummy entered the SAE corridor. Five of the six tests on dummy 077 produced a rotation that was within the specification, but all were below the minimum OC Moment. This resulted in an average, standard deviation, and CV to be calculated, but the average was below the lower bound of the OC Moment specification. None of the tests on dummy 226 produced enough rotation to meet the specification, thus the OC Moment parameter does not have an associated average, standard deviation, or CV. Likewise, a CV for reproducibility could not be calculated for the OC Moment parameter. The majority of the tests on dummy 077 matched the Mertz corridor while most of the tests on dummy 226 did not match the corridor, specifically in the peak region.

Thorax – The results for the thorax impact certification test are listed in Table 10 and the response time histories are shown in Figures 9 and 10 along with the SAE and Mertz corridors. The thorax impact responses were excellent and nearly all were within the corridor. Five of the six tests on dummy 077 and six of six tests on dummy 226 were within the SAE corridor. In addition, all of the tests matched the Mertz corridor very well.

Knee Impact – The results for the knee impact certification test are listed in Table 11 and the response time histories are shown in Figures 11 and 12 along with the SAE and Mertz corridors. The knee impact responses for both dummies were all within the SAE corridor, but most were higher than the Mertz corridor. All of the test results on dummy 226 were within the SAE corridor but all were higher than the Mertz corridor. Five of the six tests on dummy 077 were above the Mertz corridor but all were within the SAE corridor. There were some slight variations in phase for each of the dummies.

Knee Slider – The results for the knee slider certification test are listed in Table 12 and the response time histories are shown in Figures 13 through 16, along with the SAE and Mertz corridors. Nearly all of the knee slider deflections were within the SAE corridor and all very similar. Six of six tests on dummy 077 and five of six tests on dummy 226 were within the deflection corridor. All of the tests for each dummy were similar in shape and phase for the deflection responses. The knee stiffness for dummy 077 matched the Mertz corridor slightly better than dummy 226. The majority of the stiffness response for dummy 077 matched the slope of the Mertz corridors while the loading portion of the stiffness response of dummy 226 did not match the Mertz corridor.

Repeatability and Reproducibility

The traditional CV based on peak values and the time-based average CV were calculated in the manner described previously for each of the response parameters from the certification tests. If both of the dummies were repeatable, the time-based means were then compared using the t-test. If the two means were from the same population the twelve responses from both dummies were used to calculate a single time-based mean and the average CV for both dummies was calculated to assess reproducibility. If the two dummies were found to be from different populations they are considered not reproducible.

All of the repeatability and reproducibility CVs are presented in Table 13. Under the heading of Repeatability the time-based average CV and the traditional peak CV are shown. Under the heading of Reproducibility the t-statistic, the time-based average CV, and the traditional peak CV are shown. If the t-test indicated the two dummies were not from the same population the average CV was not calculated because the dummies were not reproducible. The traditional CV for peak values is presented in parenthesis although the merit of these CV values is questionable since the two dummies were found to be from different populations.

Table 5.
Dummy segment specification and actual weights

Segment Weight	Part #	Specification [kg]			Dummy 226	Dummy 077
Head Assembly	880995-1100	4.94	+/-	0.05	4.92	4.94
Neck Assembly	880995-1250	1.68	+/-	0.05	1.69	1.72
Upper Torso Assembly	880995-1300	22.3	+/-	0.36	22.0	22.5
Lower Torso Assembly	880995-1450	30.3	+/-	0.36	30.4	30.0
Upper Arm, Left	880995-700	2.81	+/-	0.09	2.79	2.83
Upper Arm, Right	880995-700	2.81	+/-	0.09	2.82	2.81
Lower Arm, Left	880995-732	2.06	+/-	0.05	2.05	2.05
Lower Arm, Right	880995-732	2.06	+/-	0.05	2.06	2.06
Hand, Left	78051-208	0.57	+/-	0.05	0.55	0.56
Hand, Right	78051-209	0.57	+/-	0.05	0.53	0.54
Upper Leg, Left	880995-1513	8.21	+/-	0.09	8.20	8.17
Upper Leg, Right	880995-1514	8.21	+/-	0.09	8.16	8.16
Lower Leg, Left	880995-1513	5.75	+/-	0.09	5.81	5.83
Lower Leg, Right	880995-1514	5.75	+/-	0.09	5.80	5.82
Foot, Left	880995-1600	1.59	+/-	0.07	1.58	1.61
Foot, Right	880995-1601	1.59	+/-	0.07	1.53	1.61
TOTAL WEIGHT		101	+/-	1.63	101	101

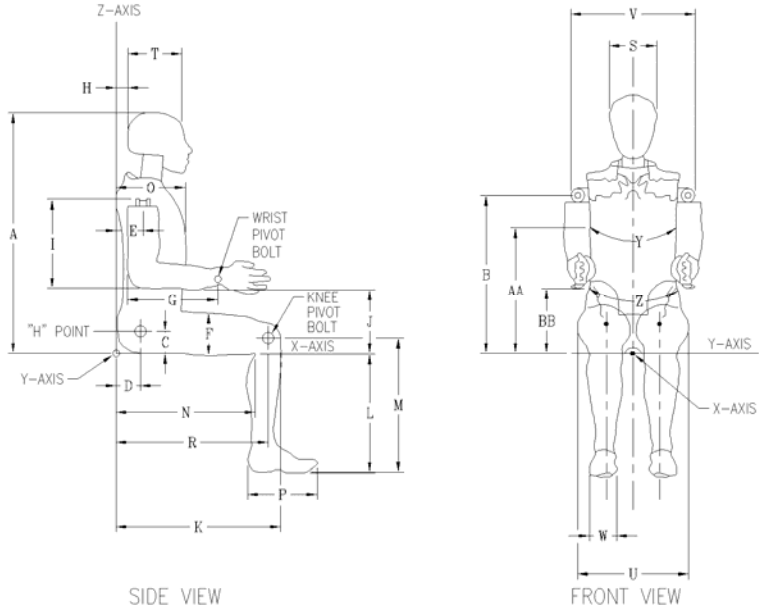

Figure 2. Reference diagram for dummy external dimensions listed in Table 6.

Table 6.
Dummy external dimension specification and actual measurements

External Dimension	Key	Specification [mm]			Dummy 226	Dummy 077
Total Sitting Height	A	919	+/-	15	921	927
Shoulder Pivot Height	B	536	+/-	15	532	541
Hip Pivot Height	C	102	+/-	5	94	97
Hip Pivot from Backline	D	155	+/-	5	142	152
Shoulder Pivot from Backline	E	91	+/-	5	97	93
Thigh Clearance	F	168	+/-	8	168	173
Back of Elbow to Wrist Pivot	G	310	+/-	8	311	312
Head Back from Backline	H	89	+/-	3	89	89
Shoulder to Elbow Length	I	363	+/-	10	356	353
Elbow Rest Height	J	213	+/-	10	210	216
Buttock to Knee Length	K	648	+/-	13	643	648
Popliteal Height	L	470	+/-	13	470	470
Knee Pivot to Floor Height	M	533	+/-	13	523	533
Buttock Popliteal Length	N	503	+/-	13	503	503
Chest Depth	O	246	+/-	8	246	246
Foot Length	P	264	+/-	8	269	264
Buttock to Knee Length	R	579	+/-	13	577	579
Head Breadth	S	155	+/-	5	160	156
Head Depth	T	196	+/-	5	201	199
Hip Breath	U	404	+/-	10	409	403
Shoulder Breath	V	475	+/-	10	472	475
Foot Breath	W	99	+/-	8	101	99
Head Circumference	X	572	+/-	5	584	574
Chest Circumference with Jacket	Y	1135	+/-	20	1130	1146
Waist Circumference	Z	1008	+/-	20	988	988
Reference Location for Chest Circumference	AA	483	+/-	5	508	508
Reference Location for waist Circumference	BB	203	+/-	5	203	203

Table 7.
Head drop certification test results for R&R

Dummy No.	Maximum Resultant Acceleration	
	220 – 265 g	
077	Average	278
	Std Dev	1.99
	%CV	0.72
226	Average	265
	Std Dev	1.03
	%CV	0.39
Both	Average	271
	Std Dev	6.95
	%CV	2.56

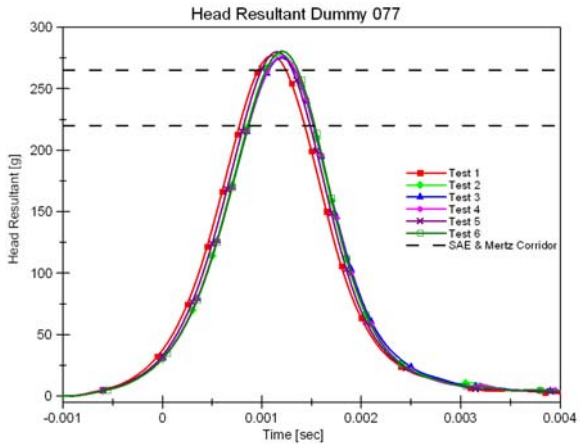

Figure 3. Dummy 077 head drop response.

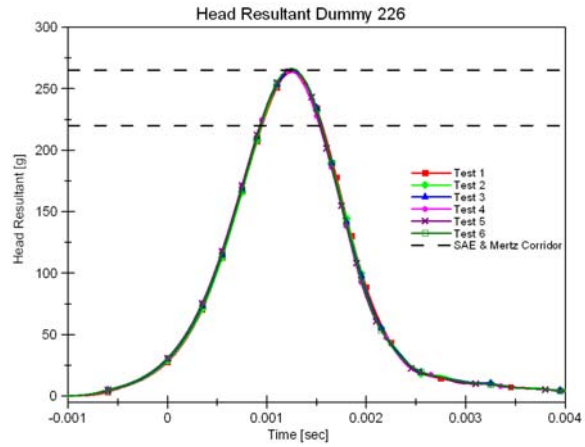

Figure 4. Dummy 226 head drop response.

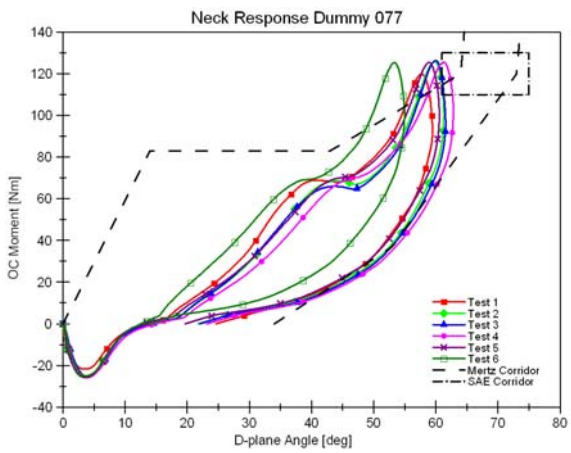

Figure 5. Dummy 077 neck flexion response.

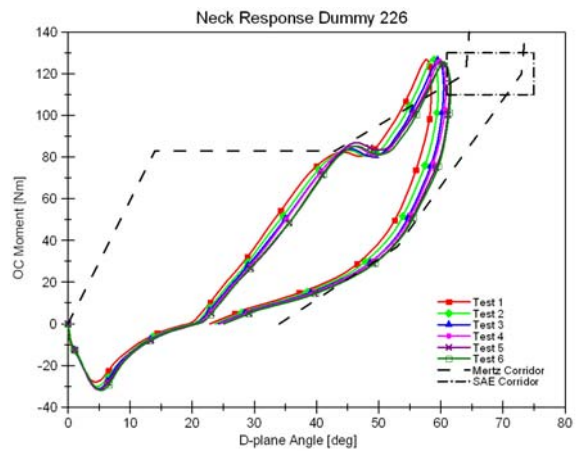

Figure 6. Dummy 226 neck flexion response.

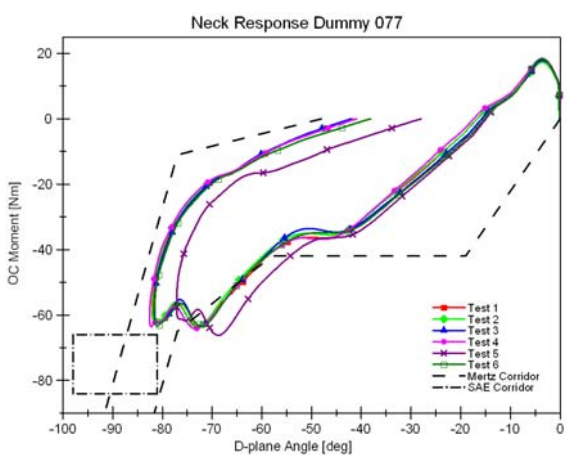

Figure 7. Dummy 077 neck extension response.

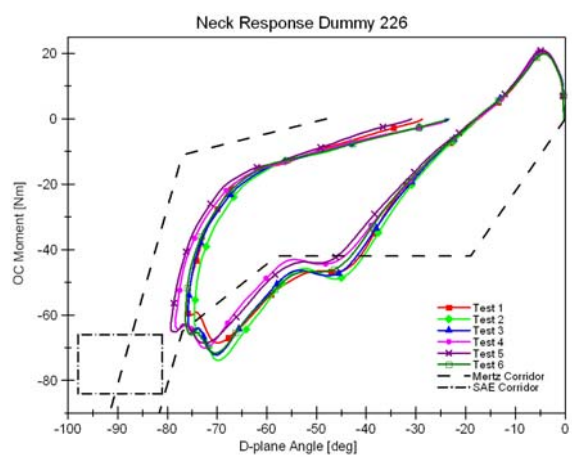

Figure 8. Dummy 226 neck extension response.

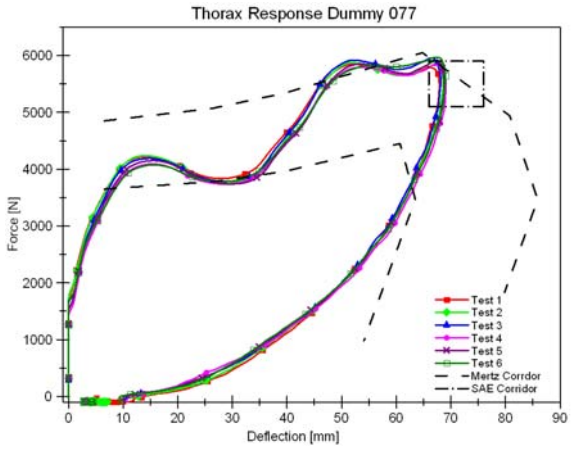

Figure 9. Dummy 077 thorax impact response.

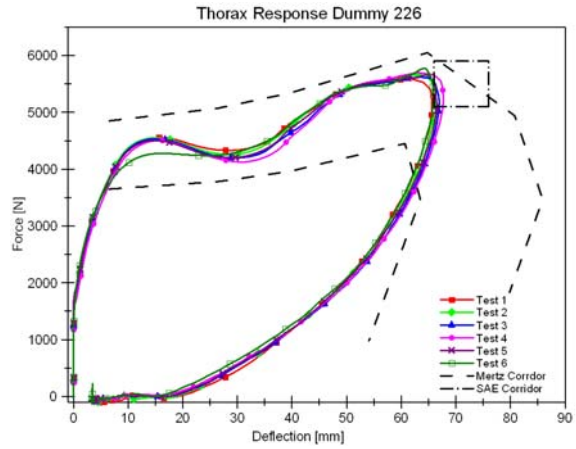

Figure 10. Dummy 226 thorax impact response.

Table 8. Neck flexion certification test results for R&R

	Impact Velocity	**Pendulum Velocity Profile**			**Peak D-Plane Rotation**	**OC Moment Peak in Rotation Interval**	**OC Moment 10 Nm Decay**	**Peak OC Moment**
	m/s	**m/s @ 10ms**	**m/s @ 20ms**	**m/s @ 30ms**	**deg**	**Nm**	**ms**	**Nm**
	6.89-7.13	**2.2-2.7**	**4.0-5.0**	**5.7-6.9**	**61-75**	**110-130**	**77-97**	
Dummy 077								
Average	6.99	2.44	4.60	6.62	62.1	123	80.3	123
Std Dev	0.00	0.01	0.03	0.04	4.60	6.31	0.35	5.72
CV %	0.00	0.56	0.75	0.60	7.40	5.13	0.44	4.63
Dummy 226								
Average	6.99	2.50	4.62	6.53	59.9	N/A	79.7	126
Std Dev	0.00	0.03	0.03	0.03	1.37	N/A	0.44	0.95
CV %	0.00	1.31	0.74	0.48	2.29	N/A	0.55	0.75
Both								
Average	6.99	2.47	4.61	6.58	61.0	N/A	80.0	125
Std Dev	0.00	0.04	0.03	0.06	3.43	N/A	0.47	4.22
CV %	0.00	1.54	0.76	0.85	5.63	N/A	0.59	3.38

Table 9.
Neck extension certification test results for R&R

	Impact Velocity	Pendulum Velocity Profile			Peak D-Plane Rotation	OC Moment Peak in Rotation Interval	OC Moment 10 Nm Decay	Peak OC Moment
	m/s	m/s @ 10ms	m/s @ 20ms	m/s @ 30ms	deg	Nm	ms	Nm
	5.95-6.91	**1.8-2.2**	**3.2-4.2**	**4.8-5.8**	**81-98**	**66-84**	**100-120**	
Dummy 077								
Average	5.96	1.93	3.69	5.32	81.2	62.5	106	64.1
Std Dev	0.02	0.02	0.03	0.05	2.02	0.90	1.48	1.10
CV %	0.41	1.22	0.74	1.01	2.49	1.45	1.39	1.72
Dummy 226								
Average	6.01	1.94	3.71	5.35	76.8	N/A	104	70.8
Std Dev	0.00	0.06	0.04	0.04	1.75	N/A	1.11	2.13
CV %	0.00	2.88	1.11	0.77	2.28	N/A	1.08	3.01
Both								
Average	5.99	1.93	3.70	5.33	79.0	N/A	105	67.4
Std Dev	0.03	0.04	0.03	0.05	2.91	N/A	1.80	3.89
CV %	0.52	2.13	0.92	0.90	3.69	N/A	1.72	5.77

Table 10.
Thorax certification test results for R&R

	Impact Velocity	Chest D_{max}	F_{max} in Defl Corridor	Hysteresis	F_{max}
	m/s	mm	kN	%	kN
	6.59 - 6.83	**66.0 - 76.0**	**5.10 - 5.91**	**69 - 85**	
Dummy 077					
Average	6.75	68.6	5.89	71.7	5.90
Std Dev	0.04	0.47	0.06	0.82	0.05
CV %	0.53	0.68	1.06	1.14	0.84
Dummy 226					
Average	6.75	66.8	5.56	73.7	5.68
Std Dev	0.01	0.74	0.10	0.52	0.05
CV %	0.15	1.11	1.86	0.70	0.90
Both					
Average	6.75	67.7	5.74	72.7	5.79
Std Dev	0.02	1.10	0.19	1.23	0.12
CV %	0.35	1.62	3.33	1.69	2.15

Table 11.
Knee impact certification test results for R&R

	Velocity	Pendulum Force
	m/S	N
	2.07 - 2.13	**4900 - 7300**
Dummy 077		
Average	2.10	6190
Std Dev	0.02	166
CV %	0.78	2.68
Dummy 226		
Average	2.10	6710
Std Dev	0.00	148
CV %	0.17	2.20
Both		
Average	2.10	6450
Std Dev	0.01	309
CV %	0.54	4.80

Table 12.
Knee slider certification test results for R&R

	Velocity	Knee Slider	Pendulum Force
	m/S	mm	N
	2.7 - 2.8	**15.0-18.3**	
Dummy 077			
Average	2.75	17.6	3710
Std Dev	0.02	0.18	86.7
%CV	0.66	1.04	2.34
Dummy 226			
Average	2.73	15.3	3920
Std Dev	0.00	0.42	36.3
%CV	0.00	2.74	0.93
Both			
Average	2.74	16.4	3810
Std Dev	0.02	1.22	129
%CV	0.62	7.39	3.38

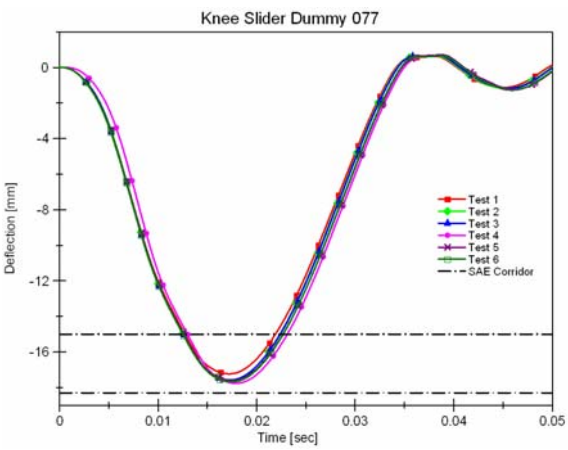

Figure 13. Dummy 077 knee slider deflection response.

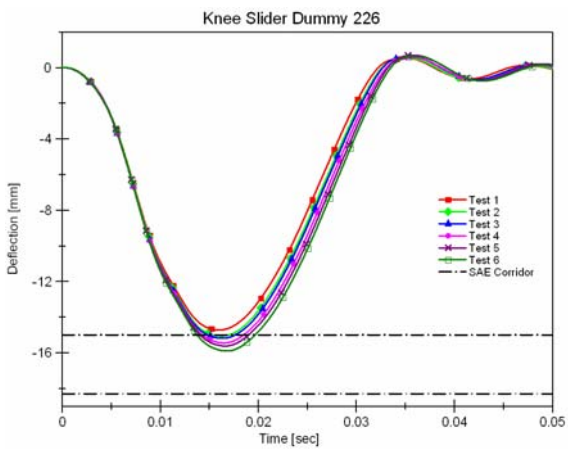

Figure 14. Dummy 226 knee slider deflection response.

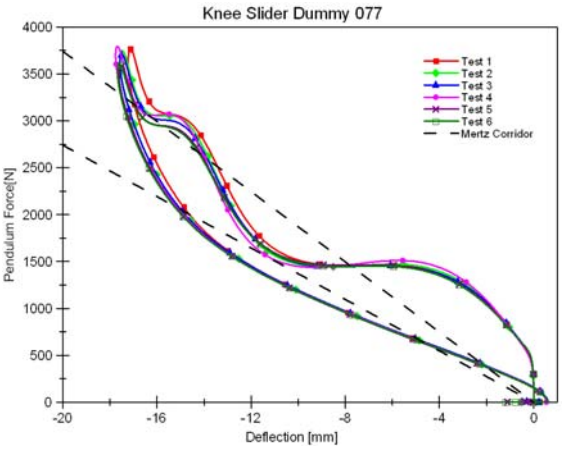

Figure 15. Dummy 077 knee slider stiffness response.

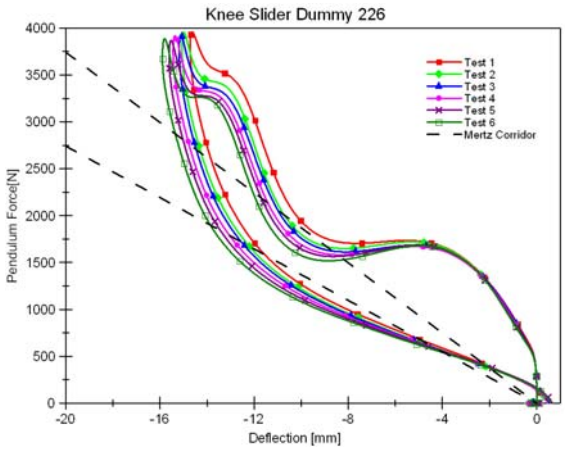

Figure 16. Dummy 226 knee slider stiffness response.

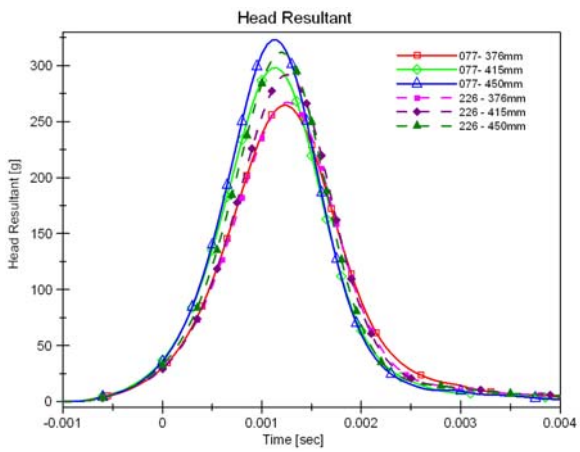

Figure 17. Head drop response for both dummies at increasing drop heights.

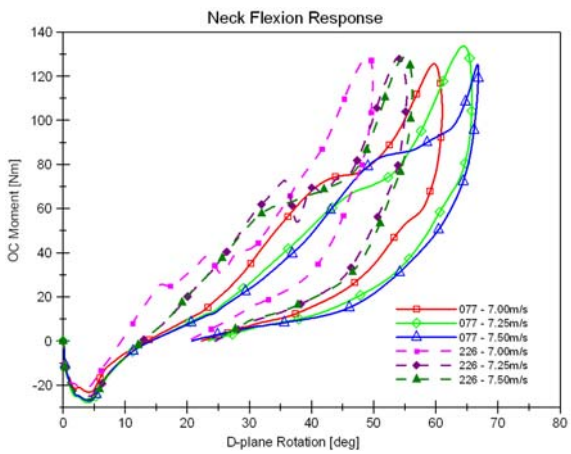

Figure 18. Neck flexion response for both dummies at increasing pendulum velocities.

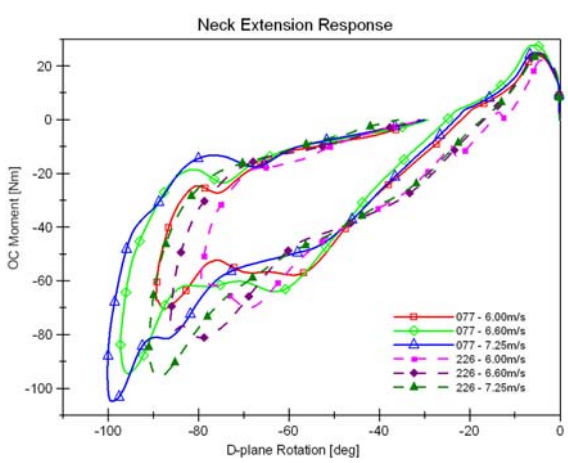

Figure 19. Neck extension response for both dummies at increasing pendulum velocities.

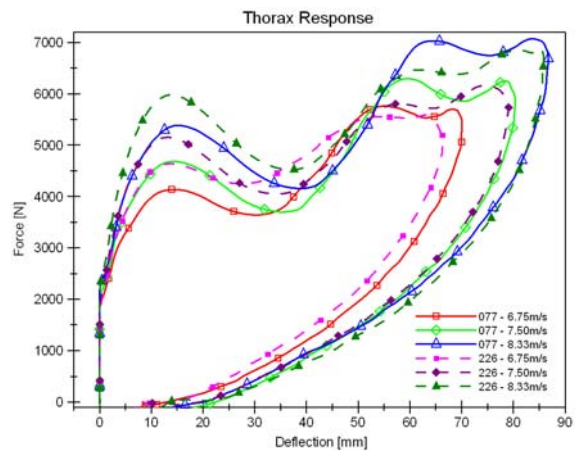

Figure 20. Thorax response for both dummies at increasing pendulum velocities.

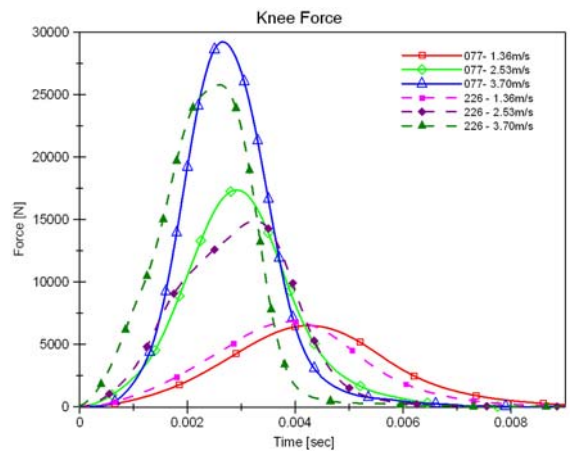

Figure 21. Knee response for both dummies at increasing 12 kg pendulum velocities.

DISCUSSION

Certification Testing

For the majority of the certification test types conducted the responses fit within the proposed SAE corridor. The tests that did not result in a response that was inside the corridor could easily be made to fit the corridor with a slight adjustment of the corridor bounds. For example, the head drop test could have the response corridor increased by 20g's and then all of the tests that were conducted would be contained within the allowable region. Likewise, the neck flexion response corridor could be moved so that the moment requirement is held the same, but the rotation requirement reduced by 7 – 10 degrees and all responses would fall within the corridor. The neck extension corridor would have to be reduced

both in terms of moment, 6 Nm, and rotation, 6 – 7 deg, so that all of the responses would fall within the corridor. The thorax and knee impact tests already fall within the corridor and would not necessitate a change. However, the knee slider deflection corridor could be reduced by 2 mm and all of the responses would be within the specification.

Repeatability and Reproducibility

In most instances the traditional approach to CV provides a lower value indicating a better repeatability or reproducibility than does the time-based average CV. This is illustrated by the knee impact force response CVs. The traditional approach results in a CV of 2.7% and 2.2% for dummy 077 and 226, respectively, while the time-based average CV results in a CV of 9.2% and 7.8% for dummy 077 and 226, respectively, nearly four times higher. This result can be explained by examining Figure 22. The six force versus time curves are relatively similar in shape, duration, and especially peak values which translates into an excellent CV value from the traditional approach. However a distinct difference in phase can be observed among the test results which is attributed to the knee itself and not the test setup (time zero defined by electrical contact switch).

Figure 23 shows the time-based average curve and plus and minus one standard deviation curves for the same six knee force responses. It can be seen that the standard deviation at the peak of the curves is smaller than at other times. Further, it can be seen that the standard deviation on the sloped sections of the curve is essentially constant. This is due to the phase shift among the curves seen in Figure 22.

Table 13.
Time series CV and peak CV comparison along with t-statistic for repeatability and reproducibility

	Repeatability			Reproducibility	
	CV Avg	**CV peaks**	**T statistic**	**CV Avg**	**CV peaks**
Head 077	4.93	0.72	2.45	6.28	2.56
Head 226	1.31	0.39			
Neck Flx Angle 077	5.77	7.40	151	4.65	5.63
Neck Flx Angle 226	2.47	2.29			
Neck Flx Mom 077	2.58	4.63	11.3	5.08	3.38
Neck Flx Mom 226	1.96	0.75			
Neck Ext Angle 077	3.53	2.49	2.91	5.94	3.69
Neck Ext Angle 226	2.76	2.28			
Neck Ext Mom 077	2.32	1.72	-17.0		(5.77)
Neck Ext Mom 226	4.12	3.01			
Thorax Force 077	2.19	0.84	56.2	3.10	2.15
Thorax Force 226	1.81	0.90			
Thorax Defl 077	1.63	0.68	17.9	1.97	1.62
Thorax Defl 226	1.58	1.11			
Knee Impact 077	9.18	2.68	-7.37		(4.80)
Knee Impact 226	7.80	2.20			
Knee Slider Defl 077	2.20	1.04	-19.0		(7.39)
Knee Slider Defl 226	3.82	2.74			
Knee Slider Force 077	3.52	2.30	-16.4		(3.38)
Knee Slider Force 226	3.50	0.93			

Coefficient of Variation <= 5%
Coefficient of Variation > 5% <= 10%
CV for dummies from different populations (#)

As a result of this situation the CV (standard deviation divided by the mean) increases as the mean value decreases and the time-based average CV is larger than the CV at the peak.

Although the knee force responses for the two dummies were both repeatable, the t-test indicates that they are not reproducible. A look at the knee force response curves of Figures 11 and 12 indicate that the two dummy knees are quite different in both magnitude and timing. The traditional CV, as shown in Table 13, is 4.8% whereas the time based average CV is 13% (not shown) which is larger than the acceptable level of 10% for reproducibility. The time-based average CV methodology is better able to identify the fact that the knee force responses are not reproducible.

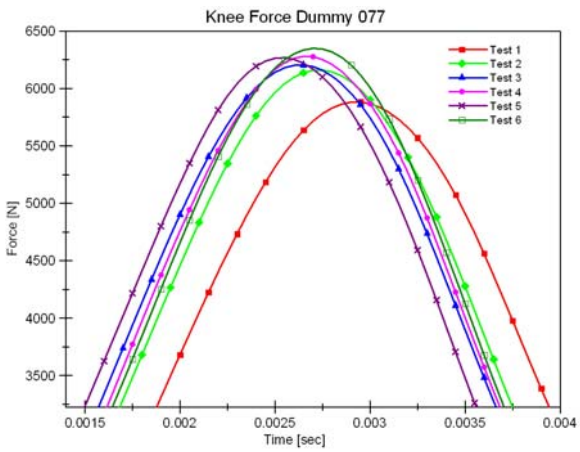

Figure 22. Knee force versus time histories near peak for dummy 077.

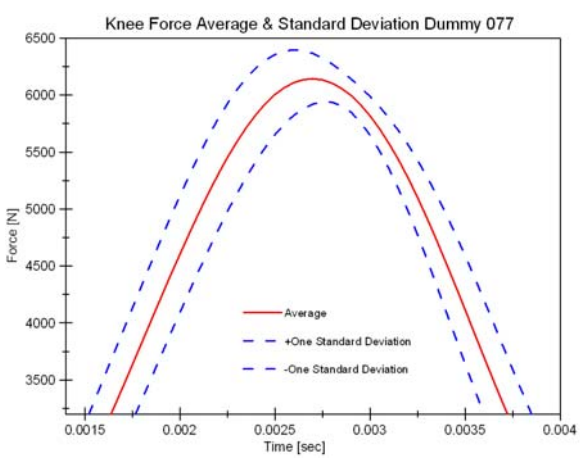

Figure 23. Knee force versus time mean and standard deviation.

Considering the other body components of these dummies that were found to be not reproducible (knee slider force and deflection and neck extension moment) the time-based average CVs (9%, 9%, 8%, respectively) are larger than the traditional CVs but the values are within the acceptable limit of 10%. This indicates that merely averaging all of the data and calculating a CV without performing the t-test does not identify non-reproducibility; the t-test is required.

CONCLUSIONS

When evaluating the averages of six repeats of the various certification tests for each dummy, it can be seen that neither dummy fully complies with the proposed SAE certification requirements. Dummy 077 does not certify with respect to the head drop requirements while dummy 265 does not certify with respect to the peak D-plane angular requirements for either neck flexion or extension. However, if the certification specifications were to be adjusted both dummies could meet the revised specifications. Because the certification specifications were based on scaled 50th percentile male specifications it is reasonable to adjust the specifications to fit the dummies so long as the dummies being evaluated are reproducible. It is to be expected that design and fabrication variances would result in a 95th sized dummy that is not a perfectly scaled replica of the 50th sized dummy.

Traditional methods of calculating repeatability CV values (CV peak method) show both dummies, individually, provide good or excellent response CVs for all of the certification tests. A proposed method of calculating a time-based CV (CV average method) also shows the CVs for both dummies to range from good to excellent although the time-based method appears to be more demanding.

The reproducibility CV is good to excellent for all certification test responses when looking at the combined data from both dummies using the traditional method of calculating CV. However, when using hypothesis testing of the time-based responses to study the reproducibility of the two dummies, the Neck Extension Moment, Knee Impact, Knee Slider Deflection, and Knee Slider Force are shown to be statistically different. If the two dummies are not from the same population the pooling of all responses from both dummies in order to calculate a CV is inappropriate.

Applying energy balance and conservation of momentum techniques to previously proposed injury

criteria for the 95th percentile large male, certification test input energy levels were increased and used to evaluate dummy durability. The head, neck, thorax, and knee from both dummies were repeatedly subjected to testing at these higher energy levels with no adverse effects observed by physical inspection or by examination of the dummy responses.

Only two dummies have been examined: one each from two manufacturers. It appears that the dummies could meet certification specifications if the current specifications were adjusted. Durability of both dummies was satisfactory even when tested at very high input energy levels. Repeatability of each of the dummies was acceptable to excellent but reproducibility of several components was less than desirable when tested using the Student t-test with a time-based tolerance of 10%.

ACKNOWLEDGEMENTS

The authors would like to thank Rick Waldeck and Ron Puckett of Transportation Research Center for their efforts in the completion of this project.

REFERENCES

Bendat, J., Piersol, A., Random Data: Analysis and Measurement Procedures, 3rd Edition, John Wiley & Sons, New York, NY. 2000.

Code of Federal Regulations, Title 49. United States Government. Washington, DC. 2004.

Mertz, H., Irwin, A., Melvin, J., Stalnaker, R., Beebe, M., "Size, Weight and Biomechanical Impact Response Requirements for Adult Size Small Female and Large Male Dummies." SAE International Congress and Exposition, Detroit, MI, 1989.

Rhule, D., Rhule, H., Donnelly, B., "The Process of Evaluation and Documentation of Crash Test Dummies for Part 572 of the Code of Federal Regulations." 19th International Technical Conference on the Enhanced Safety of Vehicles, Washington, D.C., USA, 2005.

SAE Dummy Testing Equipment Subcommittee. "User's Manual for the Hybrid III Large Male Test Dummy." Engineering Aid 26 Draft. Warrendale, PA. 2003.

EFFECT OF MUSCLE CONTRACTION ON KNEE LOADING FOR A STANDING PEDESTRIAN IN LATERAL IMPACTS

Anurag Soni
Anoop Chawla
Sudipto Mukherjee
Department of Mechanical Engineering
Indian Institute of Technology Delhi, India
Paper Number 07-0458

ABSTRACT

Knee injury thresholds are based on cadaver experiments and do not take into account active muscle contributions. Preliminary studies have indicated that muscle forces reduce injury risk in knee ligaments [Soni et al, 2006]. In this paper we study the effect of active muscle forces on knee bending angle and shear displacements for a free standing pedestrian in lateral impacts using PAM-CRASH™.

A passive FE model has been developed and validated for tests reported in Kajzer et al. (1997, 1999) and Kerrigen et al. (2003). An **A**ctive **L**ower **E**xtremity **M**odel for **S**afety (**A-LEMS**) has then been developed by including forty seven lower extremity muscles. A-LEMS has then been used to simulate below knee and ankle impacts in free standing pedestrians with activated and deactivated muscles.

The FE model shows good correlation with both Kajzer's and Kerrigan's tests results. On incorporating active muscles, it is observed that ligament strains decrease, even though the Von Mises stresses in the bones do not show a significant difference. Knee bending angle and shear displacement curves also show lower peaks with active muscles.

We conclude that muscle activation reduces ligament strains, as well as knee bending angles and shear displacements. It suggests that knee injury thresholds can be different from those formulated on the basis of cadaver studies. Therefore muscle effects should be taken into account in deciding vehicle safety standards and injury predictions in pedestrian crashes.

In this study we have assumed a straight line of action for muscles. This can lead to errors for muscles which do not work along a straight line. Tendons should also been included for more accurate muscle modeling. Currently, the study is also limited to the standing posture only and other postures are being investigated.

The current study investigates the effect of active muscle forces on the knee injury thresholds for a standing pedestrian.

INTRODUCTION

The issue of pedestrian safety has been a matter of concern for public health practitioners and vehicle designers (Ashton et al., 1977). Pedestrians represent 65% of the 1.17 million people killed annually in road accidents worldwide (World Bank, 2001). Epidemiological studies on pedestrian victims have indicated that together with the head, the lower extremities are the most frequently

injured body region (Chidester et al., 2001; Mizuno, 2003). The 2003 summary report of International Harmonized Research Activities (IHRA) Pedestrian Safety Working Group activity (Mizuno, 2003) has showed that 1,605 pedestrian victims in Australia, Germany, Japan and USA, sustained a total of 3,305 AIS 2+ injuries, out of which almost one third (32.6%) were to the lower extremity. The injuries to lower extremities in car crashes mainly include bone fractures and avulsion or stretching in knee ligaments (Mizuno, 2005). To mitigate the incidences and extent of lower limb injuries, it is essential to understand the mechanism of these injuries, and both experimental as well as numerical methods have been widely used for this purpose.

For ethical reasons, volunteer experiments cannot be performed in the higher injury severity range similar to those in pedestrian-car crashes. Therefore, the loading environment in pedestrian-car collisions has been characterized by experiments using Post Mortem Human Specimen (PMHS) (Bunketorp et al., 1981; 1983; Aldman et al., 1985; Kajzer et al., 1990; 1993; 1997; 1999; Ramet et al., 1995; Bhalla et al., 2003; 2005; Kerrigan et al., 2003; Bose et al., 2004; Ivarsson et al., 2004; 2005). As cadavers have been used in these experiments, these studies could not consider the effect of live muscle actions such as involuntary muscle reflexes, pre-impact voluntary muscle bracing etc. Mechanical legforms (the EEVC legform by TRL; FlexPLI (Konosu et al., 2005); Polar II pedestrian dummy by Honda R&D; frangible legform by Dunmore et al., 2005) have also been developed on the basis of these tests, and as a result do not account for muscle forces.

Finite element (FE) studies offer an alternate method of studying these effects. However, none of the earlier versions of validated FE models of pedestrian lower extremities (Schuster et al., 2000; Maeno et al., 2001; Takahashi et al., 2001; 2003; Matsui et al., 2001; Nagasaka et al., 2003; Chawla et al., 2004) inculde the effects of muscle actions.

Recently, Soni et al. (2006) has developed a pedestrain lower limb FE model including 40 lower extremity muscles. This model has been used to investigate the effects of pre-impact muscular contraction on knee ligament forces in lateral impacts for free standing posture of a pedestrian. Results of this preliminary investigation indicate that muscle activation decreases the probability of failure in knee ligaments.

Recently, Soni et al. (2006) has developed a pedestrain lower limb FE model including 40 lower extremity muscles. This model has been used to investigate the effects of pre-impact muscular contraction on knee ligament forces in lateral impacts for free standing posture of a pedestrian. Results of this preliminary investigation indicate that muscle activation decreases the probability of failure in knee ligaments. However, the base model used in this study has shortcomings in both geometry and material representation such as lack of bio-fidelity of base model, requirement of knee capsule, improvements needed in knee ligaments geometry, finite element selection and their material properties as reported in Chawla et al. (2004).

In the present study, we have aimed to improve our preliminary model reported in Soni et al. (2006) and then to use the improved model to study the effects of muscle contraction. Therefore, as a first step it has been decided to improve the passive response of knee joint in our basic lower extremity model developed by Chawla et al. (2004). For this purpose, geometry and material properties of knee ligaments has been modified. Knee capsule has been included as suggested by Chawla et al. (2004). Material properties of cortical as well as spongy part of bones are also modified. Then the

modified lower extremity model has been validated against the test results of Kajzer et al. (1997, 1999) and Kerrigan et al. (2003).

In the next step, Active Lower Extremity Model for pedestrain Safety (A-LEMS) has been developed. Therefore, 42 lower extremity muscles represented as 1-D bar elements are added in the validated FE model. Hill material model has been assigned to each lower extremity muscle to capture muscle contraction. A-LEMS is then used to model the standing posture of a cadaver, an aware and an unaware pedestrian. Knee bending moment, lateral shear force, knee bending angle, lateral shear displacement and strains in knee ligaments have then been compared for all three pre-impact pedestrian configurations.

FE MODEL DESCRIPTION

For the current research work, lower extremity FE model developed by Chawla et al. (2004) has been adopted as a base model. Due to the shortcomings existed in base model we have modified it to improve its response for passive loading cases.

Model Geometry

The modified model used in the present work includes the cortical and the spongy parts of the femur, tibia, fibula, and the patella. The cortical part of the bones is modeled by shell elements while the spongy part is modeled by solid elements. Apart from these, passive muscle and skin are also modeled using solid elements and membrane elements respectively. Knee ligaments, anterior cruciate ligament (ACL), posterior cruciate ligament (PCL), and lateral collateral ligament (LCL), have been modeled using solid elements. However, due to the smaller thickness in comparison to width, medial collateral ligament (MCL) has been modeled using the shell elements. To model knee ligaments, details regarding their cross-sectional areas have been taken from Takahashi et al. (2000), however, their orientations and the attachment locations on the bones have been kept similar as in our base model. Articular capsule i.e. “Knee capsule”, which encloses the knee joint and maintains joint integrity, has been included in this model. Therefore, a surface mesh enclosing the tibia plateau and the distal femur condyles has been constructed using the shell elements in HyperMeshTM.

Material Properties

Appropriate material models have been selected from the available material library of PAM-CRASH^{TM} for each part of the FE model to capture their mechanical behavior in simulation.

Spongy and the cortical parts of the bones (femur, tibia and fibula) are assumed to be isotropic elastic-plastic materials. Therefore, material models, Material # 16, and Material # 105 is used for spongy and cortical parts of the bones respectively. Takahashi et al. (2000) have done an extensive survey to determine the mechanical properties of the cortical and spongy parts of the femur and tibia. Therefore, bones mechanical properties reported in their study (listed in
Table 1) are used in our model.

Knee ligaments are assumed to behave as isotropic elastic-plastic material. Therefore, elastic-plastic material model, Material # 16 (for solid elements) is assigned to ACL, PCL and LCL, whereas Material # 105 (for shell elements) is used for MCL. Five mechanical parameters such as elastic modulus, yield stress, yield strain, ultimate stress and ultimate strain are required to charaterize the eastic-plastic behviour of knee ligaments. Values of these parameters for ACL PCL and LCL have been estimated from an experimental study conducted by Butler et al. (1986) and the similar values have been assumed for MCL. Table 2 lists the material properties assigned to knee ligaments in the FE model. Element elimination approach has been used to simulate the failure in knee ligaments. Ultimate strain value is used as the failure

threshold to initiate the element elimination process. In this process, stiffness of the element decreases to zero over 100 time steps once it is initiated. However, nodes of the eliminated elements are retained in the simulation to maintain their mass, kinetic energy, and contact properties.

Material properties of knee capsule is not available in literature, therefore material properties assigned to skin is used as an initial estimation. For the remaining lower extremity structures, material properties defined in the base model has been retained.

Table 1.

Mechanical properties of bone taken from Takahashi et al. 2001

Material Name	Density (kg/m3)	Elastic Modulus (MPa)	Yield Stress (MPa)	Yield Strain (%)	Poisson's Ratio	Ultimate Stress (MPa)	Ultimate Strain (%)
Femur Cortical	2000	14317	114.1	0.8	0.315	123.3	2.0
Tibia Cortical	2000	20033	129.0	0.63	0.315	138.1	1.5
Femur Spongy	1000	295	3.7	1.25	0.315	3.7	13.4
Tibia Spongy	1000	295	3.7	1.25	0.315	3.7	13.4

Table 2.

Mechanical properties of knee ligaments

Knee Ligaments	Density (kg/m3)	Elastic Modulus (MPa)	Yield Stress (MPa)	Yield Strain (%)	Poisson's Ratio	Ultimate Stress (MPa)	Ultimate Strain (%)
ACL, PCL, LCL, MCL	1100	345	29.8	8.64	0.22	36.4	15

FE MODEL VALIDATION FOR PASSIVE LOADING CASES

Before incorporating the muscles in the FE model it is essential to investigate the validity of the knee joint in the lower extremity model. Therefore, FE model has been validated against the PMHS test results reported by Kajzer et al. (1997, 1999) and Kerrigan et al. (2003).

Validation for Kajzer's Tests

Kajzer et al. (1997, 1999) conducted impact experiments on PMHS to load cadaver knee joints in shear and bending. These tests are intended to recreate the impact conditions usually occur in case of vehicle-pedestrian collisions. Loading and the boundary conditions used in these experiments are shown in

Figure 1.

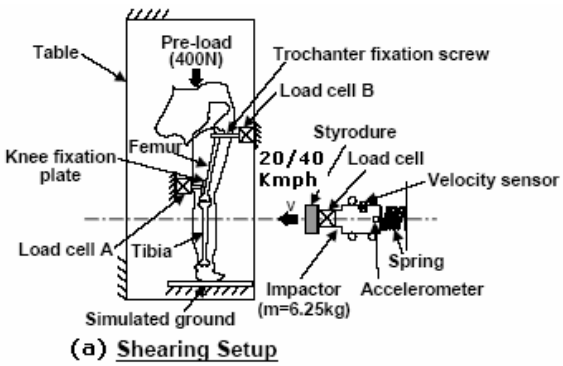

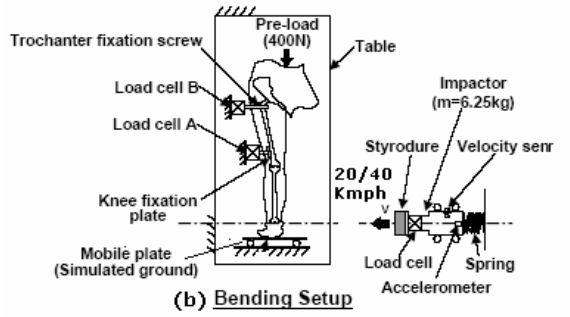

Figure 1. Kajzer's tests setup

In these tests, PMHS is laid supine on its back on the table. A plate perpendicular to the table, representing the ground, is used to support the foot of the cadaver. In case of knee shearing, foot support plate is kept fixed, whereas, in knee bending rollers are placed between the foot and the support plate to prevent the development of friction force. Preload of 400 N, corresponding to half of the body weight of a cadaver, is applied to the torso. To concentrate the impact load at the knee joint, femur is screwed at two locations. A foam covered impactor of 6.25 kg mass is propelled in lateral direction at a speed of 20 kmph and 40 kmph to impact at just below knee (shear tests) and at ankle locations (bending tests) of the leg. Wittek et al. (2000) has conducted a detailed analysis of these experiments to obtain the PMHS response corridors. These corridors have been used to validate the kinematics of knee joint in our FE model.

Experimental conditions used in Kajzer's tests have been reproduced in FE simulations. Figure 2 shows the setups used in the simulation.

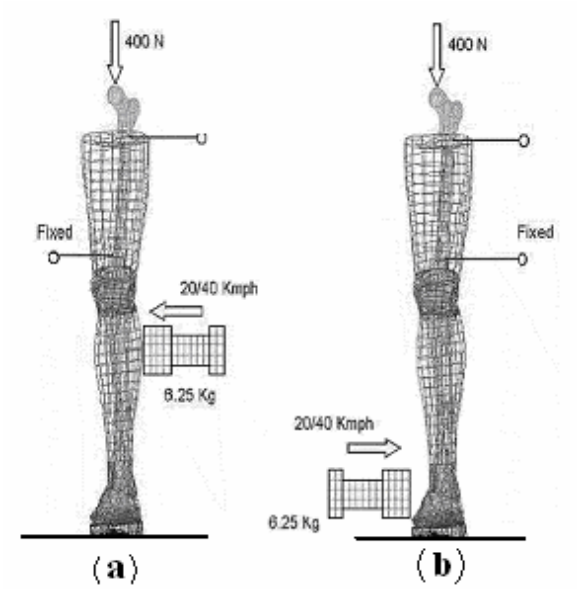

Figure 2. Simulation setup for Kajzer's tests

A rigid support plate, representing the ground in the tests, is modeled under the foot using shell elements. Coefficient of friction between the foot and support plate is kept low (0.01) in knee bending simulations to consider the effects of rollers used in bending tests. However, a relatively high value of coefficient of friction (0.3) is used in knee shearing simulations. Nodes corresponding to the upper and lower locations on the femur cortical bone are fully restrained to represent the constraints on femur in experiments. A vertical load of 400 N is applied at the top of the femur to represent the half body weight. A foam covered rigid impactor of 6.25 kg has been modeled. An initial velocity of 20 and 40 kmph has been assigned to center of gravity of the rigid impactor to propel it towards the leg. Gravity imposed acceleration field has also been modeled in all the simulations.

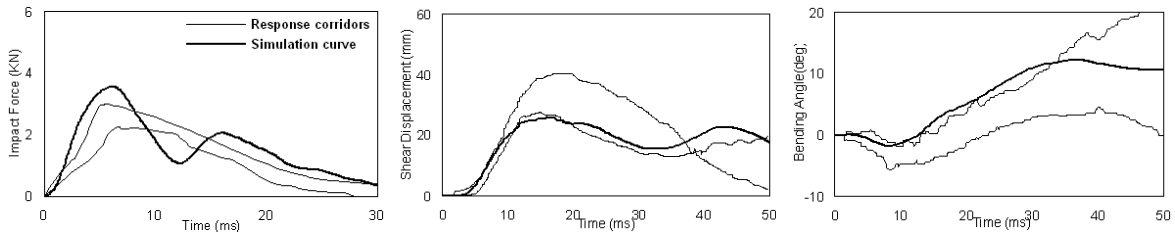

Figure 3. Comparison between PMHS response corridors and simulated impact force, shear displacement and bending angle for knee shearing at 20 Kmph

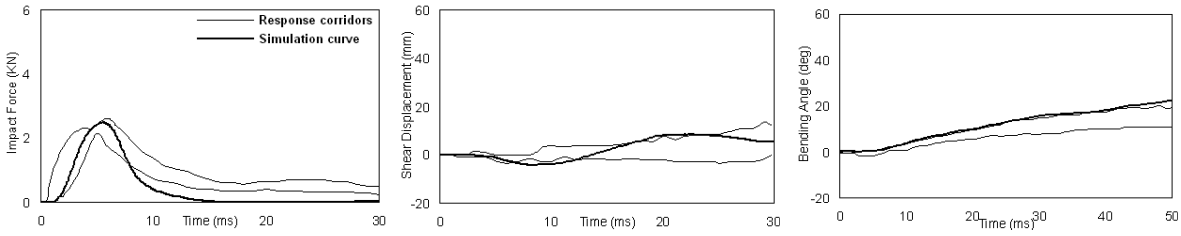

Figure 4. Comparison between PMHS response corridors and simulated impact force, shear displacement and bending angle for knee bending at 20 Kmph.

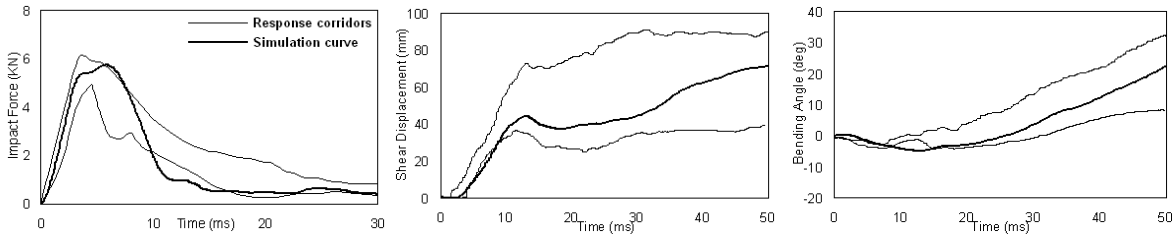

Figure 5. Comparison between PMHS response corridors and simulated impact force, shear displacement and bending angle for knee shearing at 40 Kmph.

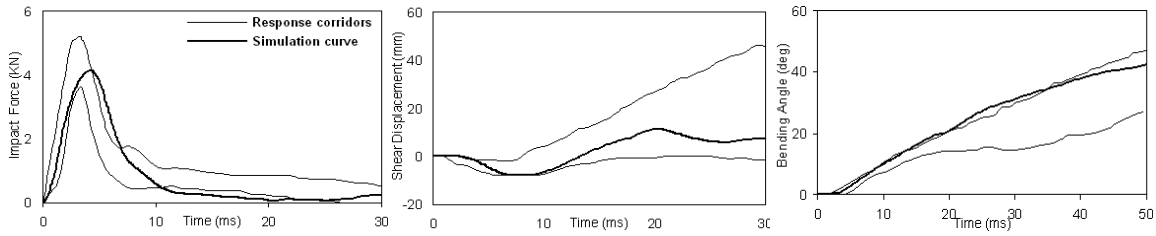

Figure 6. Comparison between PMHS response corridors and simulated impact force, shear displacement and bending angle for knee bending at 40 Kmph.

Table 3.

Injury description in shearing and bending setup at 20 Kmph for both experiment and simulation

Shearing

	Knee Ligaments			
	ACL	PCL	MCL	LCL
Simulation	☆			
Test # 21S	✹			
Test # 24S				
Test # 25S				
Test # 29S	✹			

Bending

	Knee Ligaments			
	ACL	PCL	MCL	LCL
Simulation			☆	
Test # 23B				
Test # 26B				
Test # 27B			✹	
Test # 30B			✹	

☆- Failure in simulation

✹ - Failure in experiment

Table 4.

Injury description in shearing and bending setup at 40 Kmph for both experiment and simulation

Shearing

	Knee Ligaments			
	ACL	PCL	MCL	LCL
Simulation	☆	☆	☆	
Test # 1S				
Test # 8S	✹			
Test # 16S	✹			

Bending

	Knee Ligaments			
	ACL	PCL	MCL	LCL
Simulation	☆	☆	☆	
Test # 3B		✹	✹	
Test # 6B	✹	✹	✹	
Test # 19B	✹		✹	

Figures 3-6 shows the comparison between PMHS response corridors and simulated impact force, shear displacement and bending angle for both knee shear and bending tests at 20 Kmph and 40 kmph speed. Results indicate that the simulated response of the knee joint in FE model lies within the experimental corridors. Table 3 and Table 4 summarize the comparison of knee ligament failures observed in simulations and the failure reported in the corresponding PMHS tests. The simulated failures match with the experimental failures. Thus, the lower extremity FE model validates for Kajzer's loading and boundary conditions and is capable of reproducing the failures in knee ligaments correctly.

Validation for Kerrigan's Tests

Knee joint FE model is validated against the displacement controlled dynamic four point bending and shearing tests conducted on isolated

cadaver knees in Kerrigan et al. (2003).

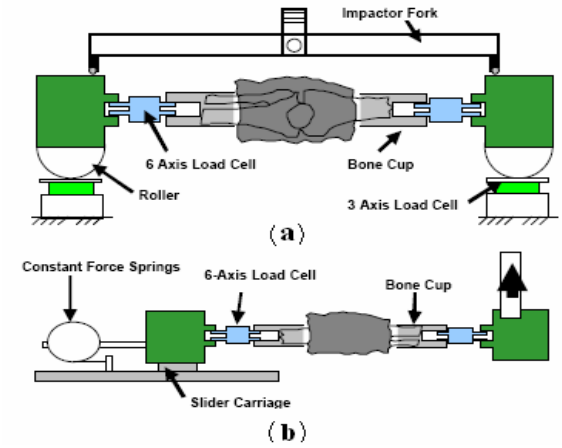

Figure 7 shows the schematics of both the experiments.

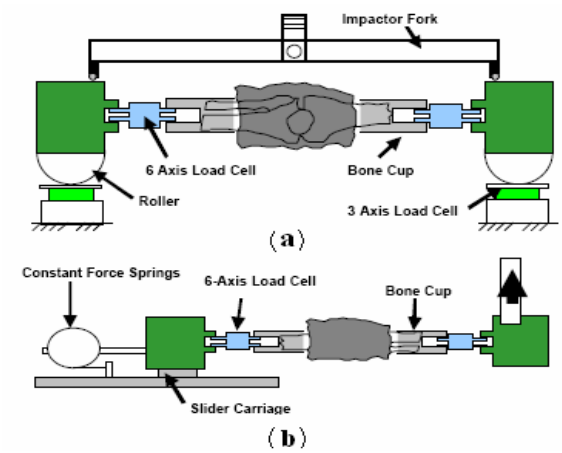

Figure 7. Schematic diagrams of dynamic (a) four point bending tests and (b) shearing tests (Reproduced from Kerrigan et al. 2003).

In four point bending tests, the end boxes are mounted on the metal rollers which are then placed on the supports. These rollers are set free to rotate in the coronal plane as well as to translate in the superoinferior direction. A twin pronged impactor is displaced with an average velocity of 0.6 m/s. Both the prongs of the impactor fork contact the inside edges of the metal end boxes and therefore push it dynamically in the lateromedial direction. As the loading locations are symmetric and are within the supporting span, this configuration has characterized the isolated cadaver knee joints in pure bending.

In knee shearing tests, the end box on the proximal side (femur side) is fixed to a slider carriage. Therefore it is only allowed to translate in the superoinferior direction. A constant force of 700 N is applied in the axial direction of the long bone. The end box on the other side (tibia side) is rigidly attached to the actuator of the displacement controlled servo-hydraulic test machine. Actuator is displaced in the lateromedial with a constant velocity of approximately 1.1 m/s. The configuration used in this test has characterized the isolated cadaver knee joints in pure shearing.

Recently, Bhalla et al. (2005b) have scaled the Kerrigan's test results (i.e. bending moment v/s bending angle and shear force v/s shear displacement plots) to the anthropometry of a 50th percentile male in order to account for the varying anthropometry of subjects tested. These scaled results have been used to validate our FE model.

Test conditions reported in Kerrigan et al. (2003) have been reproduced in FE simulations. Figure 8 shows schematic diagrams of the simulation setups representing the bending and shearing tests.

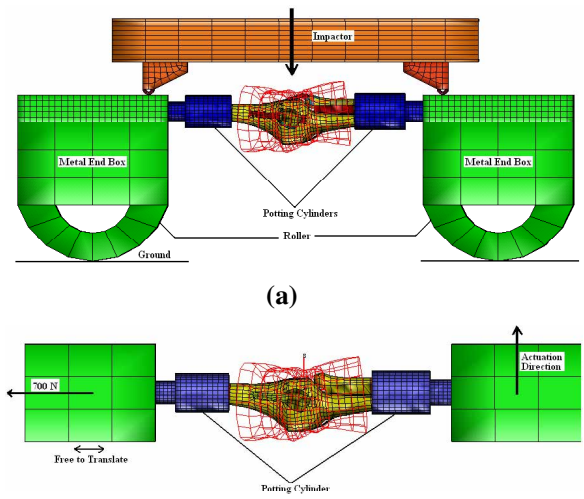

Figure 8. Simulation setup for (a) four point knee bending (b) dynamic knee shear tests performed in Kerrigan et al. (2003)

To model the test conditions, FE mesh of the knee joint including distal part of femur, proximal parts of tibia-fibula complex, knee ligaments, joint capsule, meniscus and the flesh around the knee has been segregated from our full lower extremity model. Apart from this, all the parts of the test apparatus such as potting cylinders, load cells, end boxes, metal rollers, and the twin pronged impactor are modeled using solid elements in HyperMesh™ and are defined to be rigid in simulations. In simulations, appropriate contacts are modeled between the interacting bodies

For bending simulations, center of gravity of impactor has been displaced in lateral-medial direction with a constant velocity of 0.6 m/s. The end boxes are allowed to rotate in coronal plane as well as to translate in the superioinferior direction. Two nodes at each potting cylinders have been selected to capture nodal time history plots in simulation. Relative movements of selected nodes are then used to calculate knee bending angle. A transverse plane at the center of knee joint has been defined in simulation to calculate the knee bending moment. The bending stiffness of knee model has been then compared with the bending stiffness of the cadaver knee obtained through the experiment.

In shearing simulations, the end box on the proximal side (femur side) is constrained to translate only in superoinferior direction whereas; the end box at distal side (tibia side) is displaced with a constant velocity of 1.1 m/s in lateromedial direction. A constant axial compressive force of 700 N is applied to the proximal end box. Node assigned to center of gravity of the distal end box is used to calculate the knee lateral-medial shear displacement in simulation. A transverse plane at knee center is defined to calculate the knee shear force. Shear stiffness of the knee joint model is calculated and compared with the shear stiffness of the cadaver knee obtained through the experiments.

In both bending and shearing simulations, failure occurring in knee ligaments has been compared with the ligament injuries reported in the respective experiments to assess the capability of our model in predicting the injury patterns.

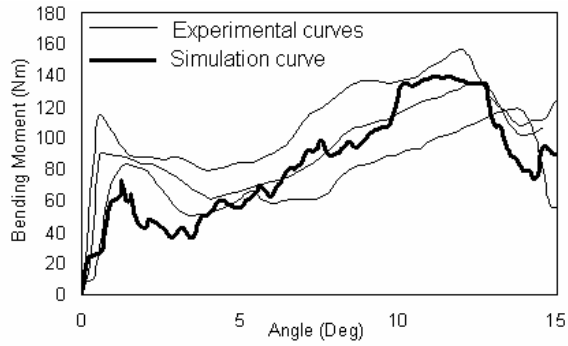

Figure 9. Comparison between simulated knee joint bending stiffness with that of obtained in cadaver experiments

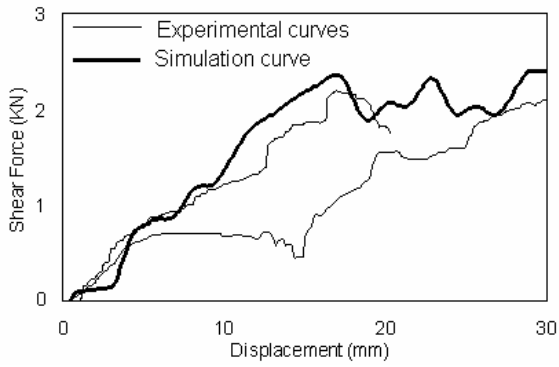

Figure 10. Comparison between simulated knee joint shear stiffness with that of obtained in cadaver experiments

Table 5.

Injury description in four point knee bending test for both experiment and simulation

	Knee Ligaments

	ACL	PCL	MCL	LCL
Simulation			☆	
Test # 1			✹	
Test # 2			✹	
Test # 3			✹	

Table 6.

Injury description in dynamic knee shear test for both experiment and simulation

	Knee Ligaments			
	ACL	PCL	MCL	LCL
Simulation	☆			
Test # 1	✹			
Test # 2	✹			
Test # 3	✹			

Figure 9 shows the comparison between the simulated and the experimental variation of knee bending moment with bending angle. Results suggest that bending stiffness of the FE knee joint is similar to that of tested cadaver knees. Table 5 gives the description of failure occurred in simulation and experiments. It is observed that MCL is the only ligament which fails in both simulations and experiments.

Similarly, Figures 10 compares the simulated and the experimental variation of knee shear force with shear displacement. Results indicate that shear stiffness of the FE knee joint is similar to that of tested cadaver knees. It is observed that ACL is the only ligament which fails in both simulations and experiments (see Table 6).

Knee joint of lower extremity FE model has been vaidated against the different sets of loading and boundary conditions reported in Kajzer et al. (1997, 1999) and Kerrigan et al. (2005). Validation results suggest that the model vaildates for all the test conditions and is also capable of reproducing the failure in knee ligaments correctly.

DEVELOPMENT OF A-LEMS

Validation of our FE model ensures its suitability for further study. Therefore, to study the effects of muscle contraction as the next course of action, 42 lower extremity muscles have been added in the validated FE model. This model has been then named as Active Lower Extremity Model for pedestrian Safety (A-LEMS).

Figure 11 shows the 42 lower extremity muscles modeled in A-LEMS.

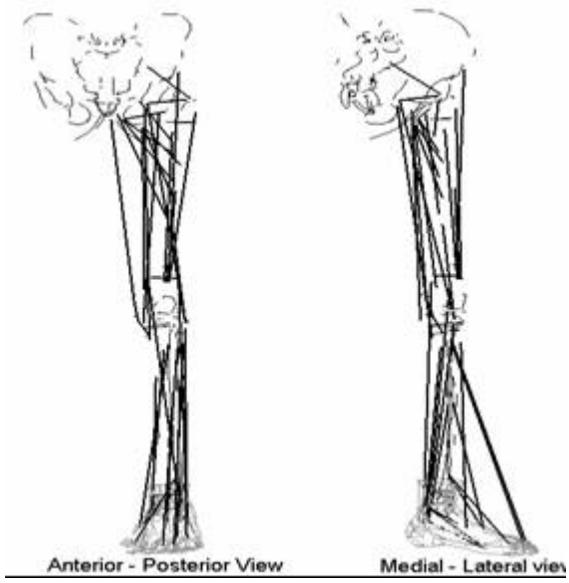

Figure 11. Anterior-posterior and Medial-Lateral views showing 42 lower extremity muscles modeled as bar elements for a standing posture. Origin and insertion location of these muscles are defined according to White et al. (1989).

Muscle Modeling

All the muscles modeled in this study is considered to exhibit straight line of action, therefore individual muscle is modeled using 1-D bar elements. Hill material model is defined for each muscle to capture its behavior in simulations.

Detailed description of muscle modeling has been provided in our previous study Soni et al. (2006). Similar approach has been followed to model the muscle to conduct the present work.

Hill Model Parameters

Muscle parameters, such as optimal muscle length (L_{opt}), maximum isometric force ($F_{\max}$), maximum contraction/ elongation velocity ($V_{\max}$), pennation angle (α), and an initial value of activation level (N_a), are required to define the Hill type muscle bar element.

Data for maximum isometric force ($F_{\max}$) and pennation angle (α) for each muscle are taken from Yamaguchi et al. (1990). Optimal muscle length (L_{opt}), at which a muscle produces maximum forces, has been adopted from Delp et al. (1980).

Maximum contraction velocity ($V_{\max}$) of a muscle depends upon the fraction of slow and fast type of fibers in it. Therefore, a muscle containing more fraction of fast type of fibers will be able to contract faster. Based on the material data available on mammalian muscles, Winters et al. (1985) has formulated an empirical relation (Equation 1) between the maximum contraction velocity of a muscle and the fraction of fast type of fibers it contains.

$$V_{\max} = 2 * Lofib(s^{-1}) + 8 * Lofib(s^{-1}) * C_{fast} \quad (1).$$

Where, L_{ofib} represents the muscle rest fiber length and C_{fast} fraction of fast fibers in a muscle.

Equation (1) has been used to calculate the maximum contraction velocity for each muscle and the data required for L_{ofib} and C_{fast} has been taken from Yamaguchi et al. (1990).

An activation level (N_a) represents the state of a muscle. It is defined as the ratio of a current force to the maximum force that can be exerted by a muscle. Thus it is a dimensionless quantity ranges from a minimum value of 0.005 to maximum value of 1. Activation value of 0.005 represents a muscle at rest whereas maximum value (i.e.1) represents maximum activation in a muscle, such as that for a maximum voluntary contraction (Winters et al., 1988).

Data used to define the Hill muscle card of each muscle in A-LEMS has been listed in Appendix A.

SIMULATIONS FOR STANDING POSTURE

Effect of muscle activation in a free standing posture of a pedestrian has been studied next. Therefore, in these simulations A-LEMS has been configured as freely standing on rigid ground plate in a gravity field. To represent the friction between road and shoe correctly, a value of 1.0 has been defined as a coefficient of friction between the shoe and ground in simulations. A 250 N load corresponding to half the body weight of a 50th percentile male minus weight of A-LEMS has been applied at the top of the femur.

Then a foam covered rigid impactor of 20 kg mass has been propelled in lateral direction at a speed of 25 kmph to impact A-LEMS at two locations i.e. below-knee and at-ankle. Bhalla et al. (2005a) has reported that for a 50th percentile male, centerline of the car bumper hits the lower leg 45 mm below the tibia plateau. Therefore to reproduce the real world vehicle-pedestrian impact conditions for below knee impact, we have also positioned the impactor such that the center line of impact should be 45 mm below the of tibia plateau. Whereas, for ankle impact, impactor is positioned such that it should hit the ankle at its center.

Figure 12 shows the simulation setups for both below-knee and at-ankle impact.

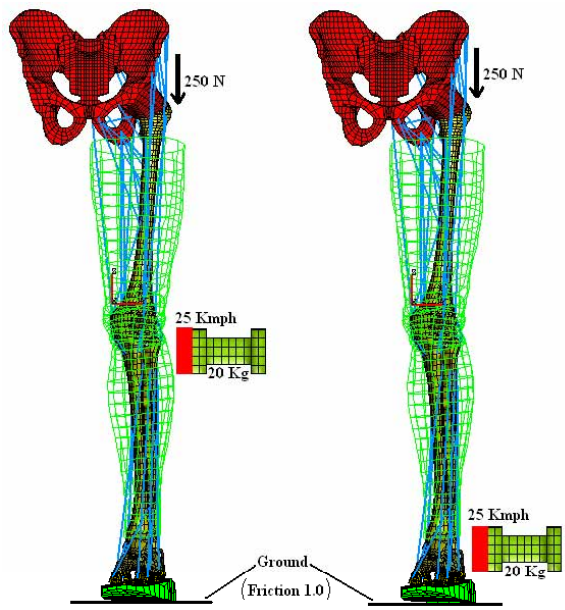

Figure 12. Simulation setups for below knee and ankle impact.

Three sets of simulations (S1, S2, and S3) have been performed for each impact location. In each set of simulation, muscles in A-LEMS have been modeled such that it represents a different pre-impact configuration of a pedestrian occur in real world.

In S1, a quiet standing pedestrian who is unaware of an accident has been simulated. Therefore, to model A-LEMS for this simulation, initial muscle activation level required to maintain the stability of a standing posture of a pedestrian in gravity field are assigned in Hill muscle card of each muscle using data reported by Kuo et al. (1993). These activation values are listed in Table A1 in appendix A. A stretch based invlountery reflex action has also been enabled in this simulation. This is to include the ability of live activated muscle to contract against a small stretch produced by an outside agency. In medical terms this kind of reflex action is known as "stretch reflex". A threshold elongation value has been defined in Hill material cards to trigger the stretch reflex in a muscle in simulation

Ackerman, (2002) has suggested a delay of 20 ms for the onset of involuntary reaction for skeletal muscles. This delay mainly represents time taken by the signal to travel through the central nervous system (CNS) circuitry. Therefore, a delay of 20 ms is assigned in Hill material card to onset the involuntary reflexive action after a muscle gets triggered for stretch reflex.

In S2, a standing pedestrian who is aware of an accident has been simulated. To model this configuration bracing in muscles has been considered. In bracing a muscle is fired at its full capacity and no signal flows from spinal cord to muscle. Therefore, to represent bracing action, all the muscles have been assigned a maximum value of 1 as an initial muscle activation level. Apart from this, reflexive action is also set off.

In S3, a standing cadaver has been simulated. This configuration has been modeled by assigning minimum value of 0.005 as an initial muscle activation level in all the muscles in A-LEMS and reflexive action has also been kept off.

Two nodes at both femur and tibia have been selected to obtain the nodal time history in simulations. Relative movements of selected nodes are then used to calculate knee bending angle and shear displacement. A transverse plane at the center of knee joint has been defined in simulations to calculate bending moment and lateral shear force. Springs of very low stiffness are modeled on each knee ligament to calculate strain time history in simulations. However, element elimination approach has also been enabled to simulate the failure in knee ligaments. Response of S1, S2 and S3 has been then compared to determine the role of muscle loading.

RESULTS AND DISCUSSION

The loading can be divided into two phases. In the initial phase, the impactor contacts the lower extremity which is initially at rest and passes energy in-elastically to the leg segments. Relative movement between tibia and femur starts only after the impactor force crosses a certain threshold, leading to fall in impactor contact force and a shear loading in the knee joint.

In the second phase, the motion of the lower extremity creates a bending motion at the knee joint called varus and valgus. The large angular displacement between femur and tibia due to this bending motion leads to stretching in ligaments and the ligament forces peak during this phase.

Below Knee Impact

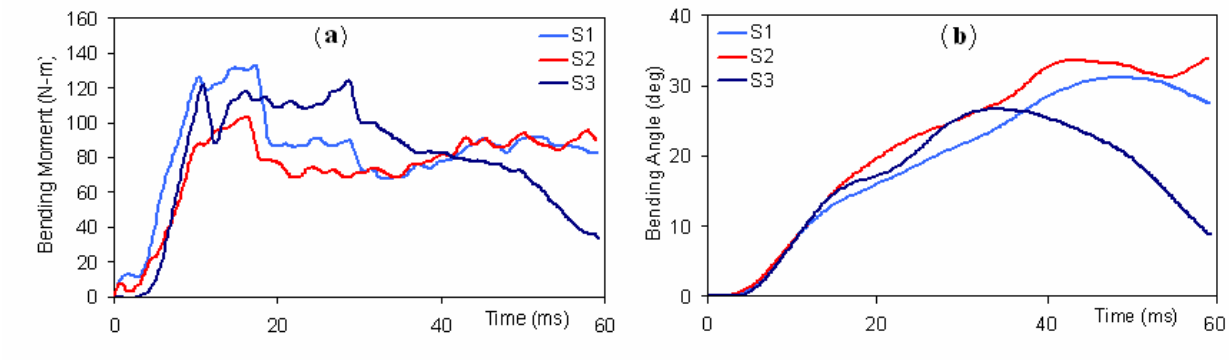

Figure 13. Comparison of (a) bending moment time history and (b) bending angle time history for three configurations (S1, S2 and S3) of a freely standing pedestrian in below-knee impact

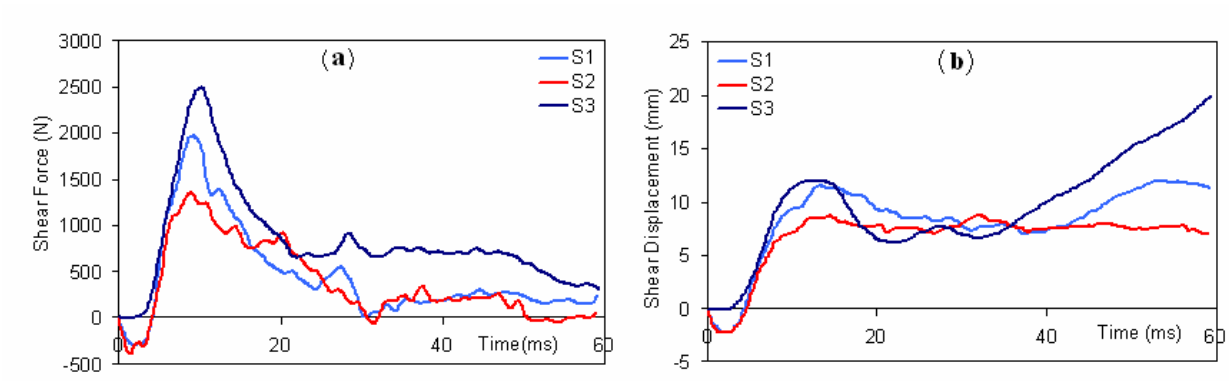

Figure 14. Comparison of (a) shear force time history and (b) shear displacement time history for three configurations (S1, S2 and S3) of a freely standing pedestrian in below-knee impact

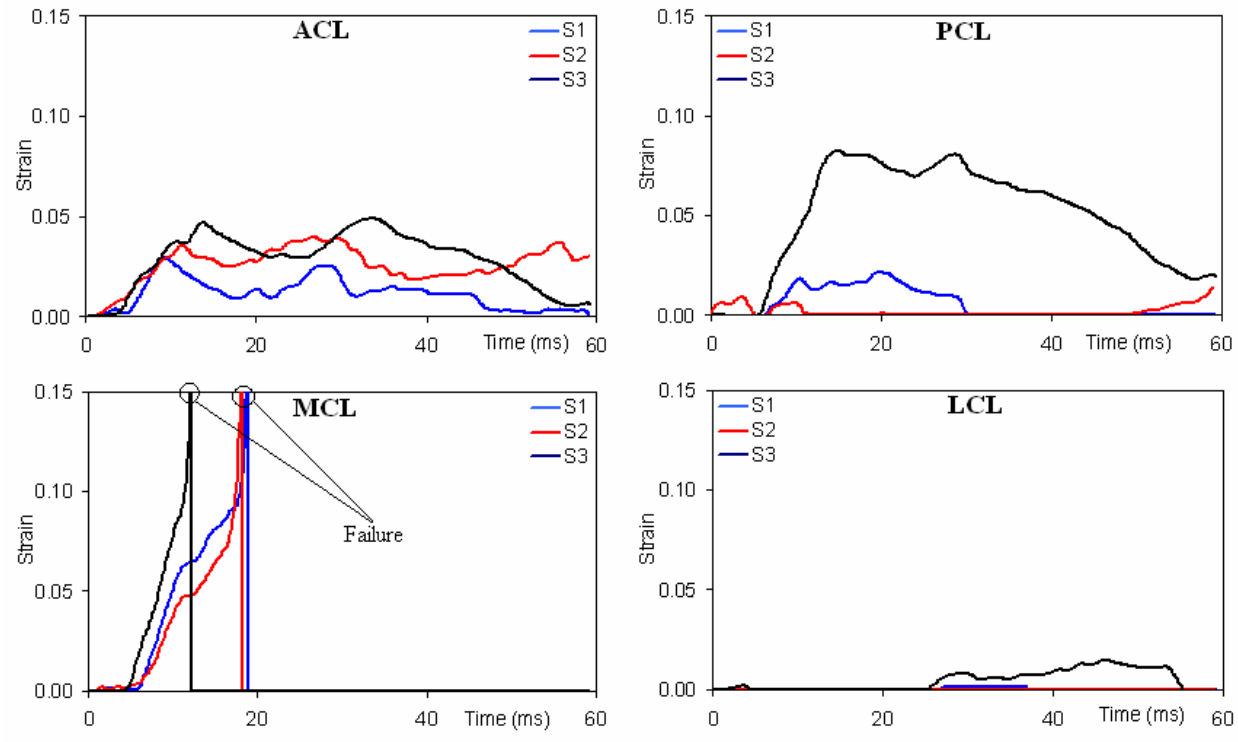

Figure 15. Comparison of strain time histroy in knee ligaments for three configurations (S1, S2 and S3) of a freely standing pedestrian in below-knee impact

Ankle Impact

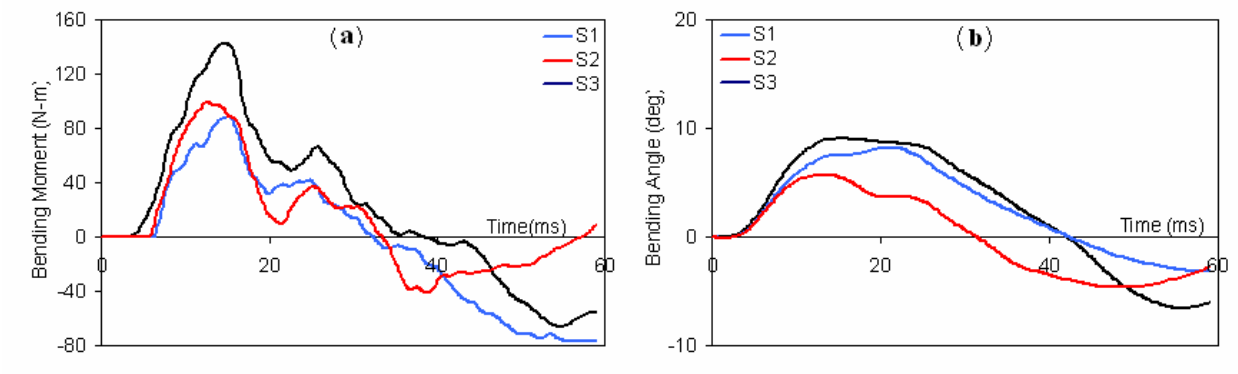

Figure 16. Comparison of (a) bending moment time history and (b) bending angle time history for three configurations (S1, S2 and S3) of a freely standing pedestrian in ankle impact

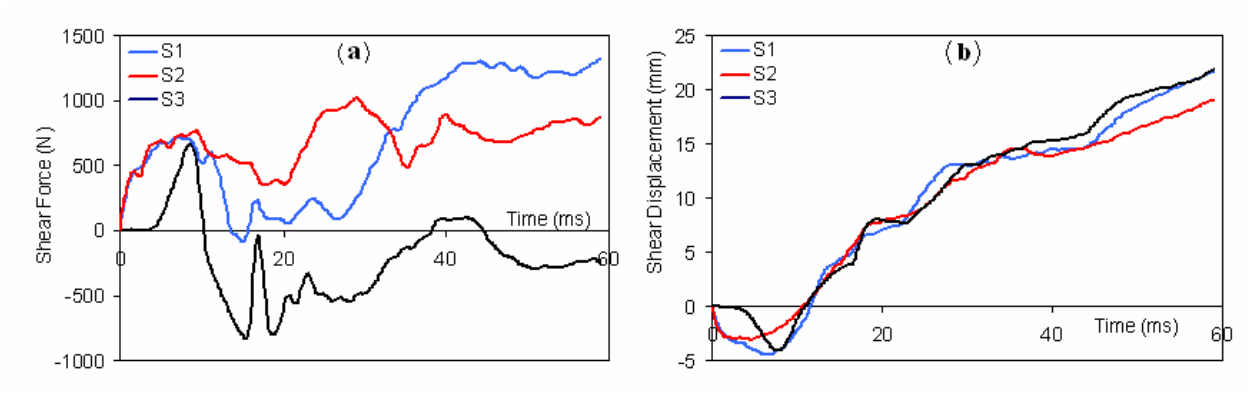

Figure 17. Comparison of (a) shear force time history and (b) shear displacement time history for three configurations (S1, S2 and S3) of a freely standing pedestrian in ankle impact

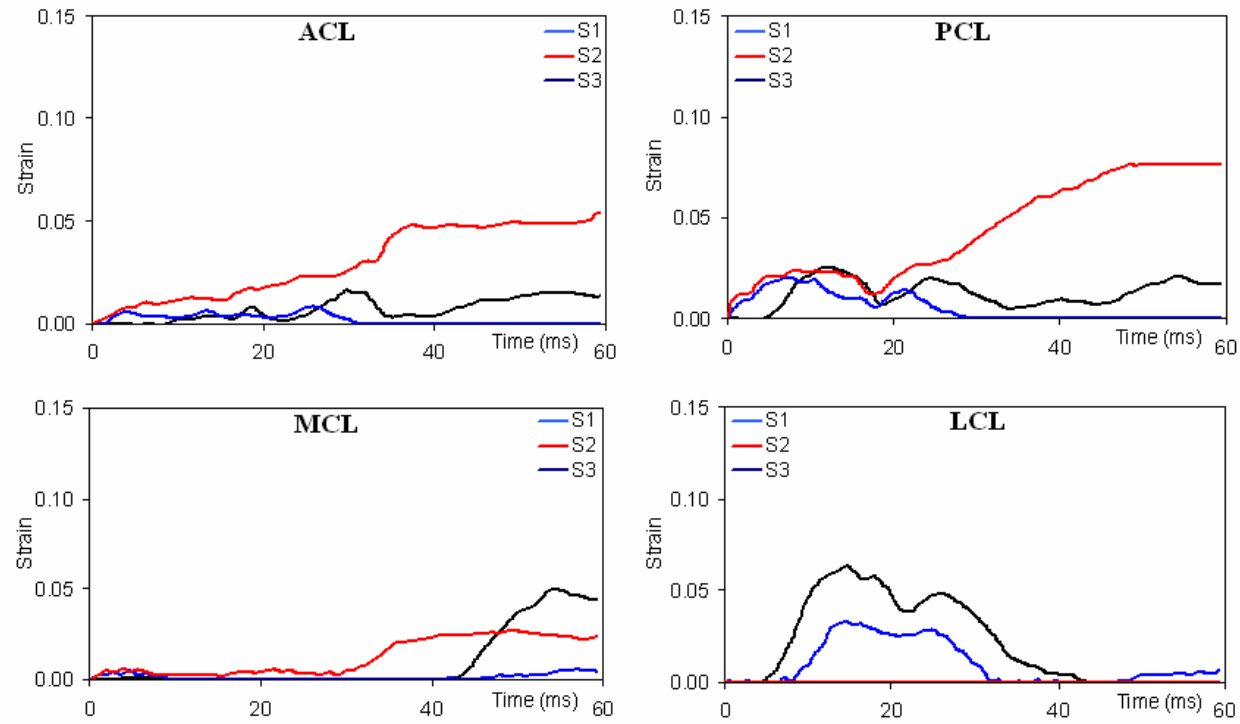

Figure 18. Comparison of strain time histroy in knee ligaments for three configurations (S1, S2 and S3) of a freely standing pedestrian in ankle impact

CONCLUSION

LIMITATIONS AND FURTHER IMPROVEMENTS

In our study, the data for point of origin and insertion was from White et al., (1989). The basis for selection of this study was the similarity in the height of the reported male specimen (177 cm) and THUMS (AM50) (175 cm), there is still a difference of 2 cm in their body height. According

to Winter et al (2005) the length of the lower extremity segment is on the average 0.53 times the total body height. Using this estimate, the difference in the lower extremity segments is about 1 cm. This difference can be further reduced by using scaling techniques. Dimensions of individual segments (femur, tibia, fibula and pelvis) required to calculate scaling factors in each direction, were not available in the literature. Apart from this, THUMS represents a 50th percentile American male and its segments length are not according to the standard fraction of total body height. However, we do not anticipate that a difference of 1 cm in length of lower extremities will change the results significantly.

In the present study we have adopted a straight line geometric model of the muscle because of the simplicity of definition using the origin and insertion locations of a muscle. This approach can lead to errors for muscles which do not work in a straight line (gracilis, semitendinosis, tibialis posterior, flexor digitorium longus, flexor hallucis longus, tibialis anterior, extensor hallucis longus, extensor digitorium longus, peroneus tertius, peroneous brevis, and peroneus longus). Multiple points could be used in the muscle definition to account for the curved path of some muscles.

For further improvements in the current finite element model, tendons should also be modeled along with the muscles to consider their effects.

Present model considers only the upper body mass; however the inclusion of its detailed geometry may affect the kinematics of knee joint.

ACKNOWLEDGEMENTS

The authors would like to acknowledge the support from the Transportation Research and Injury Prevention Program (TRIPP) at Indian Institute of Technology Delhi and the Volvo Research Foundation. The authors also acknowledge Toyota Central Research and Development Lab (TCRDL) for providing the finite element human body model, Total Human body Model for Safety (THUMS) which has been used in this study.

REFERENCES

1. Ackerman U., PDQ Physiology (2002) Ch. (2), at, www.fleshandbones.com/readingroom/pdf/226.pdf
2. Aldman, B., Kajzer, J., Bunketorp, O., Eppinger, R. (1985) An experimental study of a modified compliant bumper. In Proceedings of 10th International Technical Conference on the Experimental Safety Vehicles.
3. Ashton, S., J., Pedded, J., B., Mackay, G., M. (1977) Pedestrian injuries, the bumper and other front structure. International IRCOBI conference on the Biomechanics of Impact, pp.33-51.
4. Bhalla, K., Bose, D., Madeley, N.,J., Kerrigan, J., Crandall, J., Longhitano, D., and Takahashi, Y. (2003) Evaluation of the response of mechanical pedestrian knee joint impactors in bending and shear loading, In Proceedings of the 2003 ESV conference.
5. Bhalla, K., Takahashi, Y., Shin, J., Kam, C., Murphy, D., Drinkwater, C., J., Crandall. (2005a) Experimental investigation of the response of the human lower limb to the pedestrian impact loading environment. Society of Automotive Engineers World Congress, SAE paper, 2005-01-1877
6. Bhalla, K., Bose, D., Madeley, N. J., Kerrigan, J., Crandall, J., Longhitano D., Takahashi, Y., (2005b), Evaluation of the response of mechanical pedestrian knee joint

impactors in bending and shear loading, Proceeding of the 2005 ESV conference.

7. Bose, D., Bhalla, K., Rooij, L., Millington, S., Studley, A., and Crandall, J., (2004) Response of the knee joint to the pedestrian impact loading environment. SAE paper number 2004-01-1608.
8. Bunketorp, O. et al., (1981) Experimental studies on leg injuries in car-pedestrian impacts. IRCOBI, pp.243-255.
9. Bunketorp, O. et al., (1983) Experimental study of a compliant bumper system. SAE Paper Number 831623.
10. Butler D L, Kay M D, Stouffer D C. (1986) Comparison of material properties in fascicle bone units from human patella tendon and knee ligaments. J. Biomechanics, Vol. 19, pp. 425-432
11. Chawla, A., Mukherjee, S., Mohan, D. and Parihar, A. (2004) Validation of lower extremity model in THUMS. IRCOBI.
12. Chidester, A. B., Isenberg, R. A. (2001) Final report - the pedestrian crash data study. In Proceedings of the 17 International Technical Conference on the Enhanced Safety of Vehicles.
13. Dunmore, M., Brooks, R., McNally, D., Madeley, J., (2005). Development of an alternative frangible knee element for a pedestrian safety legform. In proceedings of 2005 IRCOBI Conference.
14. Ivarsson, J., Lessley, D., Kerrigan, J., Bhalla, K., Bose, D., Crandall, J., Kent, R., (2004) Dynamic response corridors and injury thresholds of the pedestrian lower extremities. In Proceedings of 2004 IRCOBI Conference.
15. Ivarsson, J., Kerrigan, J., Lessley, D., Drinkwater, C., Kam, C., Murphy, D., Crandall, J., Kent, R. (2005) Dynamic response of corridors of the human thigh and leg in non midpoint three-point bending. Society of Automotive Engineers World Congress, SAE paper, 2005-01-0305
16. Kajzer, J., Cavallero, S., Ghanouchi, S., Bonnoit, J., (1990) Response of the knee joint in lateral impact: Effect of shearing loads. IRCOBI.
17. Kajzer, J., Cavallero, S., Bonnoit, J., Morjane, A., Ghanouchi, S., (1993) Response of the knee joint in lateral impact: Effect of bending moment. IRCOBI.
18. Kajzer, J., Schroeder, G., Ishikawa, H., Matsui, Y., Bosch, U. (1997) Shearing and Bending Effects at the Knee Joint at High Speed Lateral Loading. Society of Automotive Engineers, SAE Paper 973326.
19. Kajzer, J., Ishikawa H., Matsui Y., Schroeder G., Bosch U. (1999) Shearing and Bending Effects at the Knee Joint at Low Speed Lateral Loading. Society of Automotive Engineers, SAE Paper 1999-01-0712.
20. Kerrigan, J., Bhalla, K., Madeley, N., Funk, J., Bose, D., Crandall, J. (2003) Experiments for establishing pedestrian impact lower injury criteria. SAE Paper 2003-01-0895.
21. Konosu A., Issiki, T., Tanahashi M. (2005) Development of a biofidelic flexible pedestrian leg-form impactor (Flex -PLI 2004) and evaluation of its biofedility at the component level and the assembly level. Society of Automotive Engineers World Congress, SAE paper, 2005-01-1879.
22. Kuo, A. D. and Zajac, F. E. (1993) A biomechanical analysis of muscle strength as a limiting factor in standing posture. Journal of Biomechanics 26, 137-150.
23. Maeno, T. and Hasegawa, J. (2001) Development of a finite element model of the total human model for safety (THUMS) and

application to car-pedestrian impacts. 17th international ESV conference, Paper No. 494.

24. Matsui, Y. (2001) Biofidelity of TRl legform impactor and injury tolerance of human leg in lateral impact. Stapp Car Crash Journal, Vol 45
25. Mizuno, Y. (2003) Summary of IHRA Pedestrian safety WG activities (2003) – proposed test methods to evaluate pedestrian protection afforded by passenger cars. In Proceedings of the 18th International Technical Conference on the Enhanced Safety of Vehicles.
26. Mizuno, Y. (2005) Summary of IHRA Pedestrian safety WG activities (2005) – proposed test methods to evaluate pedestrian protection afforded by passenger cars. In Proceedings of the 19th International Technical Conference on the Enhanced Safety of Vehicles.
27. Nagasaka, K., Mizuno, K., Tanaka, E., Yamamoto, S., Iwamoto, M., Miki, K. and Kajzer J. (2003) Finite element analysis of knee injury in car-to-pedestrian impacts. Traffic injury prevention, 4:345-354.
28. Ramet, M., Bouquet, R., Bermond, F., Caire, Y. (1995) Shearing and Bending Human Knee Joint Tests In Quasi-Static Lateral Load. Proceeding of the International Conference on the Biomechanics of Impact (IRCOBI).
29. Schuster, J. P., Chou, C. C., Prasad, P.,Jayaraman, G. (2000) Development and validation of a pedestrian lower limb non-linear 3-D finite element model. 2000-01-SC21, Vol. 44. Stapp Car Crash journal.
30. Soni A, Chawla A, Mukherjee S. (2006) Effect of muscle active forces on the response of knee joint at low speed lateral impacts. Society of Automotive Engineers World Congress, SAE paper, 2006-01-0460
31. Takahashi, Y., Kikuchi, Y. Konoso, A., Ishikawa, H., (2000) Development and validation of the finite element model for the human lower limb of pedestrians, Proceedings of 44th Stapp Car Crash Conference, Paper 2000-01-SC22.
32. Takahashi, Y., Kikuchi, Y. (2001) Biofidelity of test devices and validity of injury criteria for evaluating knee injuries to pedestrians, Proceedings of the ESV conference.
33. Takahashi, Y., Kikuchi, Y., Mori, F., Konosu, A. (2003) Advanced FE lower limb model for pedestrians. 18th International ESV conference, Paper no. 218.
34. White, S. C., Yack, H. J. and Winters, D. A. (1989) A three dimensional musculoskeletal model for gait analysis, anatomical variability estimates. Journal of Biomechanics 22, 885-893.
35. Wittek, A., Ishikawa, H., Matsui, Y., Konosu, A., (2000) Validation and parameter study of a multibody model for simulation of knee joint responses in lateral impacts representing car-pedestrian accidents: Influences of ligament properties and boundary conditions on model responses. Proceedings of IRCOBI conference, Montpellier, France, pp. 85-99.
36. World Bank (2001) Road Safety, http://www.worldbank.org/transport/roads/safety.html
37. Yamaguchi, G., Sawa, A., Moran, D., Fessler, M. and Winters, J. (1990) A survey of human musculotendon actuator parameters. In: Winters, J. Woo, S., (Eds.) Multiple Muscle Systems, Springer, New York pp. 717-773.

APPENDIX - A

42 lower extremity muscles are defined in the local reference frames according to White et al. (1989). Data used to define Hill muscle card for a muscle are listed in the Table A.1.

Table A.1.

Data for Lower extremity muscles

Muscle	F_{max} (N)	L_{opt} (mm)	C_{fast}	aV_{max} (Ratio of V_{max} to L_{opt})	N_a
Vastus Lateralis	1871	0.084	0.52	5.85	0.005
Vastus Intermedius	1365	0.087	0.5	5.10	0.005
Vastus Medialis	1294	0.089	0.53	5.36	0.005
Rectus Femoris	779	0.084	0.619	5.55	0.005
Soleus	2839	0.03	0.25	2.67	1*
Gastrocnemius Medialis	1113	0.045	0.518	5.74	1*
Gastrocnemius Lateralis	488	0.064	0.518	5.69	1*
Flexor Hallucis Longus	322	0.043	0.5	5.17	0.005
Flexor Digitorium Longus	310	0.034	0.5	4.58	0.005
Tibialis Posterior	1270	0.031	0.5	4.65	1*
Tibialis Anterior	603	0.098	0.27	3.28	0.5*
Extensor Digitorium Longus	341	0.102	0.527	5.31	0.005
Extensor Hallucis Longus	108	0.111	0.5	4.32	0.005
Peroneus Brevis	348	0.05	0.375	4.59	1*
Peroneus longus	754	0.049	0.375	4.35	0.005
Peroneus Tertius	90	0.079	0.375	4.76	0.005
Biceps Femoris (LH)	717	0.109	0.331	3.55	1*
Biceps Femoris (SH)	402	0.173	0.331	3.91	1*
Semimembranosus	1030	0.08	0.5	5.61	1*
Semitendinosus	328	0.201	0.5	4.76	1*
Piriformis	296	0.026	0.5	5.71	0.005
Pectineus	177	0.133	0.5	4.62	0.005
Obturatorius Internus	254		0.5	5.71	0.005
Obturatorius Externus	109		0.5	5.71	0.005
Gracilis	108	0.352	0.5	5.13	0.005
Adductor Brevis 1	286	0.133	0.5	5.17	0.005
Adductor brevis 2	286	0.133	0.5	5.22	0.005
Adductor Longus	418	0.138	0.5	4.69	0.5*
Adductor Mangus 1	346	0.087	0.416	5.07	0.005
Adductor Mangus 2	444	0.121	0.416	5.07	0.005
Adductor Mangus 3	155	0.131	0.416	5.07	0.005
Glutaeus Maximus 1	382	0.142	0.476	5.53	0.005
Glutaeus Maximus 2	546	0.147	0.476	5.53	0.005
Glutaeus Maximus 3	368	0.144	0.476	5.53	0.005
Glutaeus Medius 1	546	0.054	0.5	5.71	0.005
Glutaeus Medius 2	382	0.084	0.5	5.71	0.005
Glutaeus Medius 3	435	0.065	0.5	5.71	0.005
Glutaeus Minimus 1	180	0.068	0.5	5.71	0.005

Glutaeus Minimus 2	190	0.056	0.5	5.71	0.005
Glutaeus Minimus 3	215	0.038	0.5	5.71	0.005
Sartorius	104	0.579	0.504	5.03	0.005
Tensor Fasciae Latae	155	0.095	0.5	5.71	1*

* - Na represents initial activation level in a muscle during standing posture. These values have been taken from Kuo et al., (1993).